State-selective control for vibrational excitation and dissociation of diatomic molecules with shaped ultrashort infrared laser pulses

M. V. Korolkov,[a] G. K. Paramonov,[a] and B. Schmidt
Institut für Physikalische und Theoretische Chemie, WE 3, Freie Universität Berlin, Takustrasse 3, D-14195 Berlin, Germany

(Received 25 October 1995; accepted 26 April 1996)

Ultrafast state-selective dynamics of diatomic molecules in the electronic ground state under the control of infrared picosecond and femtosecond shaped laser pulses is investigated for the discrete vibrational bound states and for the dissociative continuum states. Quantum dynamics in a classical laser field is simulated for a one-dimensional nonrotating dissociative Morse oscillator, representing the local OH bond in the H_2O and HOD molecules. Computer simulations are based on two approaches — exact treatment by the time-dependent Schrödinger equation and approximate treatment by integro-differential equations for the probability amplitudes of the bound states only. Combination of these two approaches is useful to reveal mechanisms underlying selective excitation of the continuum states and above-threshold dissociation in a single electronic state and for designing optimal laser fields to control selective preparation of the high-lying bound states and the continuum states. Optimal laser fields can be designed to yield almost 100% selective preparation of any prescribed bound state, including those close to the dissociation threshold. State-selective preparation of the highest bound state may be accompanied by the appearance of a quasi-bound molecular state in the continuum with the kinetic energy of the fragments being close to zero. The respective above-threshold dissociation spectrum contains an additional, zero-order peak. The laser-induced dissociation from selectively prepared high-lying bound states is shown to be very efficient, with the dissociation probability approaching the maximal value. Flexible tools of state-selective laser control are developed which enable one to achieve selective control of the dissociation spectra resulting in time-selective and space-selective control of the dissociation fragments. © *1996 American Institute of Physics.* [S0021-9606(96)02729-8]

I. INTRODUCTION

Selective excitation and dissociation of molecules by laser radiation is a subject of considerable interest in recent years.[1–5] It constitutes a wide field of investigations resulting in many fundamental applications ranging from collision dynamics to molecular spectroscopy and laser chemistry.[6–10] An important line in this field is selective control of molecular dynamics by properly designed laser fields. Selective steering a molecule to a specified target may result in various types of intermolecular and intramolecular selectivity including, in particular, isotope-selectivity,[3] mode-selectivity,[11–14] state-selectivity,[15–25] wave packet focusing on electronic surface,[26–29] narrowband inversion of population,[30] laser-controlled isomerization[31–33] and related isotope separation.[34] The respective optimal laser pulse shaping techniques have been a topic of much interest recently.[35–44] They may be based, for example, on optimal control theory (OCT),[35] as developed by Rabitz and co-workers,[36–41] they may employ the individual optimization of one[15–17,19] or more[21,31–34] laser pulses with arbitrary shapes, adiabatic passage control schemes with optimal timing of pulse sequences,[22–25] control of the frequency sweep in broadband laser pulses,[30] or make use of chirped laser pulses.[43,44]

In this work we consider the laser-controlled state-selective molecular preparation at specified high vibrational levels, up to the dissociation threshold, in the electronic ground state on a femtosecond (fs) and picosecond (ps) time scale, along with the laser-induced dissociation from selectively prepared states. Until now, high vibrational levels have not been a target for ultra-fast state-selective excitation. State-selective vibrational excitation in the electronic ground state has been simulated for low vibrational levels of several diatomic and triatomic molecules,[19–21,44–49] neglecting the laser-induced coupling of the discrete bound states to the dissociative continuum states. At the same time, in theoretical studies of the laser-induced dissociation (see, e.g., Refs. 50–54) a molecule is often considered to be already prepared selectively at a certain vibrational level, neglecting the preparation itself, which can obviously be accompanied by substantial dissociation if no care is taken of optimal design of the laser field preparing the state. This is especially important for very high vibrational states, close to the dissociation threshold. At the same time, it is most desirable to prepare a molecule selectively specifically in high vibrational states. This creates favourable starting conditions for efficient dissociation and for controlling the state-selective excitation of the continuum as well. Besides the laser-induced dissociation, ultrafast state-selective preparation of molecules at high vibrational levels is useful for subsequent chemical reactions, for controlling cross-sections in molecular collisions, and for spectroscopic studies.

[a]Permanent address: B. I. Stepanov Institute of Physics, Belarus Academy of Sciences, Skaryna ave. 70, 220602 Minsk, Republic of Belarus.

In the present work we bridge the gap between the state-selective preparation and controlled state-selective dissociation of diatomic molecules. In the first stage, our aim is to achieve maximal, close to 100%, state-selectivity for the preparation of high vibrational bound states up to the very top ones, along with minimization of the dissociation probability. In the second stage, we use shaped infrared laser pulses of fs/ps duration for controlling molecular dissociation from the selectively prepared high-lying bound states. Our goal in this stage is to achieve maximal dissociation probability along with controllable localization of population in narrow energy domains of the continuum. The ultimate aim is state-selective steering of a molecule to any specified target in the discrete and continuum spectra.

An alternative approach[41] includes efficient multiphoton dissociation by the OCT-designed laser pulse sequences from the vibrational ground state. However, the state-selective laser control of molecular dynamics both in the potential well and in the continuum was not specified as a target in Ref. 41. In earlier works (see, e.g., Refs. 50–54) simulations were carried out for rectangular pulses, which are not suitable for state-selective control of molecular dynamics on a fs/ps time scale, or shaped laser pulses were not properly optimized (see, e.g., Ref. 55) and they did not yield appreciable state-selectivity.

The most straightforward approach to the problem at hand is direct numerical solution of the time-dependent Schrödinger equation. Alternative, approximate methods, which may use complex, non-Hermitian effective Hamiltonians (CEH), or various L^2 discretized continuum schemes, have been discussed in detail in Ref. 53.

In our present work, the quantum dynamics of an isolated nonrotating diatomic molecule is treated by the time-dependent Schrödinger equation for the wave function $\Psi(r,t)$ as well as by the respective equations of motion for the probability amplitudes, where the laser induced transitions between the continuum states are neglected. The latter treatment follows in part the approach of Flosnik and Wyatt.[53] Combination of the two approaches proved to be suitable for revealing mechanisms underlying selective excitation of the continuum states, for analysing the processes of above-threshold dissociation in a single electronic state, and for designing optimal laser fields controlling selective preparation of the bound and continuum states.

As a model system in our simulations we use a dissociative, one-dimensional Morse oscillator, with the specific parameters representing the local OH bond in the H_2O and HOD molecules, which is an extension of the previous investigations[19–21] where dissociation was neglected. Rotations are not taken into account. The interaction with the laser field is treated semiclassically: quantum molecule in classical electric field, which for intense laser fields has been shown to be numerically equivalent to the fully quantum treatment.[56] Atomic units are used unless otherwise explicitly indicated.

II. MODEL, EQUATIONS OF MOTION AND TECHNIQUES

The OH bond under study is specified by the molecular Hamiltonian

$$\mathscr{H}_{\rm mol}=p^2/2m+V_M(r), \tag{1}$$

with the reduced mass m and Morse potential

$$V_M(r)=D\{\exp[-\beta(r-r_0)]-1\}^2-D, \tag{2}$$

where the equilibrium distance $r_0=1.821a_0$, Morse parameter $\beta=1.189a_0^{-1}$, and well depth $D=0.1994$ hartree.

The discrete, bound molecular eigenstates are denoted as $|v\rangle$. The molecular Hamiltonian $\mathscr{H}_{\rm mol}$ supports 22 bound vibrational eigenstates with the respective eigenenergies

$$E_v=-D+\hbar[\omega_e(v+0.5)-\Delta^a(v+0.5)^2], \tag{3}$$

where $v=0,1,\ldots,V=21$, the harmonic frequency $\omega_e=\beta\sqrt{2D/m}$, and the anharmonicity constant $\Delta^a=\hbar\omega_e^2/4D$. The eigenfunctions $\psi_v(r)$ of bound states are well-known Morse oscillator wave functions (see, e.g., Refs. 57 and 58).

The continuum eigenstates with eigenenergies $E>0$ are denoted as $|E\rangle$, and the eigenfunctions $\psi(E,r)$ of the continuum states may be represented by the Whittaker functions (see, e.g., Ref. 59).

The molecular eigenstates satisfy the time-independent Schrödinger equations

$$\mathscr{H}_{\rm mol}(r)|v\rangle=E_v|v\rangle, \quad \mathscr{H}_{\rm mol}(r)|E\rangle=E|E\rangle \tag{4}$$

and the orthonormalization relations

$$\langle v|v'\rangle=\delta_{vv'}, \quad \langle E|E'\rangle=\delta(E-E'), \quad \langle E|v\rangle=0. \tag{5}$$

The interaction of OH with a linearly polarized laser field is described within the semiclassical electric dipole approximation by the interaction Hamiltonian

$$\mathscr{H}_{\rm int}(r,t)=-\mu(r)\mathscr{E}(t), \tag{6}$$

where $\mathscr{E}(t)$ is the component of the electric field strength along the molecular dipole, and the molecular dipole moment operator is described by Mecke function[60,61]

$$\mu(r)=\mu_0 r\ \exp(-r/r^0) \tag{7}$$

with $\mu_0=7.85$D/Å and $r^0=0.6$ Å.

The quantum dynamics of OH in the laser field $\mathscr{E}(t)$ is described by the time-dependent Schrödinger equation

$$i\hbar\frac{\partial}{\partial t}\Psi(r,t)=[\mathscr{H}_{\rm mol}(r)+\mathscr{H}_{\rm int}(r,t)]\Psi(r,t). \tag{8}$$

Initially, at $t=0$, the OH is supposed to be in the vibrational ground state. The time-dependent Schrödinger equation (8) is solved by a split time propagation (STP) method,[62–64] with the fast Fourier transform procedure used at each grid point. The time step of propagation Δt ranges from 1 to 3 atomic time units. The spatial grid parameters are $\Delta r=0.06\ a_0$ and $r_n=n\Delta r$ for $n=1,2,\ldots,N$ with $N=1024,2048,4096$ and 8192. The Morse potential (2) is cut off at $r=\Delta r$. At the end of the grid, the wave function $\Psi(r,t)$ is damped using a ''gobbler'' technique with a Gaussian-shaped function.[65] In

fact, in the present simulations the damping is practically avoided during the state-selective preparation and dissociation of a molecule because of the very large value of r_N. This is checked by the norm remaining on the grid,

$$\mathcal{N}(t)=\int_{\Delta r}^{r_N} dr\Psi(r,t)^*\Psi(r,t), \tag{9}$$

which always fulfils $\mathcal{N}(t)=1$ with much better than 1% accuracy. The extended grids (large r_N) are also important in order to achieve a good resolution in momentum space. The continuum contribution to the overall wave function $\Psi(r,t)$ is evaluated in configuration space as

$$\Psi_{\rm cont}(r,t)=\Psi(r,t) - \sum_{v=0}^{V} \psi_v(r)\int_{\Delta r}^{r_N} dr'\psi_v(r')^*\Psi(r',t), \tag{10}$$

and in momentum space as

$$\Phi_{\rm cont}(K,t)=(2\pi)^{-1/2}\int_{\Delta r}^{r_N} dr\Psi_{\rm cont}(r,t)\exp(-iKr). \tag{11}$$

The dissociation probability is defined as

$$\mathcal{D}(t)=\int_{\Delta r}^{r_N} dr|\Psi_{\rm cont}(r,t)|^2. \tag{12}$$

The time-dependent Schrödinger equation (8) is the first basic equation of motion in the present work, which will be refered to as the STP approach.

In the second approach the time-dependent wave function is represented in the basis of bound ($|v\rangle$) and continuum ($|E\rangle$) states. The respective equations of motion for the probability amplitudes $a_v(t)$ and $a(E,t)$, where the laser-induced continuum–continuum transitions are neglected, are derived following Flosnik and Wyatt[53] as follows. The time-dependent wave function $\Psi(r,t)$ is expressed in the interaction picture as

$$\Psi(r,t)=\sum_{v=0}^{V} a_v(t)\exp(-i\omega_v t)|v\rangle+\int_0^\infty dE a(E,t) \times\exp(-i\omega_E t)|E\rangle, \tag{13}$$

where $E_v=\hbar\omega_v$ and $E=\hbar\omega_E$, while $a_v(t)$ and $a(E,t)$ are the probability amplitudes for the bound and the continuum states, respectively. Substituting Eq. (13) into Eq. (8) and operating, as usual, with $\langle v|\exp(i\omega_v t)$ and $\langle E|\exp(i\omega_E t)$ yields, after neglecting the continuum-continuum transitions, the infinite set of coupled differential equations

$$i\hbar\frac{d}{dt}a_v(t)=-\mathscr{E}(t)\sum_{v'=0}^{V}\langle v|\mu|v'\rangle\exp(i\omega_{vv'}t)a_{v'}(t) - \mathscr{E}(t)\int_0^\infty dE\langle v|\mu|E\rangle\exp(i\omega_{vE}t)a(E,t), \tag{14}$$

and

$$i\hbar\frac{d}{dt}a(E,t)=-\mathscr{E}(t)\sum_{v'=0}^{V}\langle E|\mu|v'\rangle\exp(i\omega_{Ev'}t)a_{v'}(t), \tag{15}$$

where $\omega_{vv'}=\omega_v-\omega_{v'}$ and $\omega_{Ev'}=\omega_E-\omega_{v'}$. The initial conditions are

$$a_v(t=0)=\delta_{v0}, \quad a(E,t=0)=0 \tag{16}$$

for the bound and the continuum states, respectively.

The formal solution of Eq. (15) with the initial conditions (16) has the form

$$a(E,t)=(i/\hbar)\sum_{v'=0}^{V}\langle E|\mu|v'\rangle\int_0^t dt'\mathscr{E}(t') \times\exp(i\omega_{Ev'}t')a_{v'}(t'). \tag{17}$$

Substitution of Eq. (17) into the right-hand side of Eq. (14) yields the following $(V+1)$-dimensional set of integro-differential equations (IDE) for the discrete bound states only:

$$i\hbar\frac{d}{dt}a_v(t)=-\mathscr{E}(t)\sum_{v'=0}^{V}\langle v|\mu|v'\rangle\exp(i\omega_{vv'}t)a_{v'}(t) -(i/\hbar)\mathscr{E}(t)\exp(i\omega_v t)\sum_{v'=0}^{V}\int_0^{E_{\max}}dE \times\int_0^t dt'\langle v|\mu|E\rangle\langle E|\mu|v'\rangle\exp(-i\omega_E t) \times\mathscr{E}(t')\exp(i\omega_{Ev'}t')a_{v'}(t'), \tag{18}$$

where the upper limit of integration over the continuum energy E is set to $E_{\max}$ which is detailed below. The initial conditions are $a_v(t=0)=\delta_{v0}$.

The IDE (18) is the second basic equation of motion in the present work in addition to the time-dependent Schrödinger equation (8). It allows the quantum molecular dynamics to be evaluated in terms of the bound states only and is refered to as the IDE approach. Further approximations to the IDE (18), similar to those of Flosnik and Wyatt,[53] proved not to be acceptable here, because of the fast oscillations of the probability amplitudes $a_v(t)$ in strong laser fields.

The dipole moment matrix elements for bound–bound transitions $\langle v|\mu|v'\rangle$ are evaluated from Eq. (7) following methods developed in Ref. 58. A similar approach is used here for evaluating the matrix elements for bound–continuum transitions $\langle v|\mu|E\rangle$, which can be reduced to tabulated integrals[66] (details are given in the Appendix). Suffice it to indicate here that in our model of OH a strong decrease of the bound–continuum coupling with increasing energy at $E>0.05$ D allows in our model of OH the upper limit of integration over the continuum energy E in the IDE (18) to be chosen as $E_{\max}<0.5$ D, with the specific value depending on the laser field strength and the carrier frequency.

The integrals over E in the IDE (18) are approximated with sums, assuming that the $\langle v|\mu|E\rangle$ are approximately constant over a series of energy intervals

$[E_{(i)}, E_{(i)}+\Delta E_{(i)}]$, where $\Delta E_{(i)}$ are adjusted to obtain desired accuracy. The size of each energy interval $\Delta E_{(i)}$ depends on the behavior of the dipole matrix elements $\langle v|\mu|E\rangle$ in the vicinity of the discretized continuum energy $E_{(i)}$. The IDE (18) can be solved by using straightforward modifications of standard numerical methods.[67] The solution $a_v(t)$ of the IDE (18) yields the populations of the vibrational bound states

$$P_v(t)=|a_v(t)|^2. \tag{19}$$

We shall also use the overall population of all bound states

$$P_{\text{well}}(t)=\sum_{v=0}^{V} P_v(t), \tag{20}$$

and the state-selectivity

$$\mathscr{S}_v(t)=P_v(t)/P_{\text{well}}(t) \tag{21}$$

of the molecular preparation in the bound state $|v\rangle$.

As soon as the probability amplitudes $a_v(t)$ of the bound states are obtained from the IDE (18), the continuum ones $a(E,t)$ are evaluated from Eq. (17). The populations of the continuum states are represented in our work by integrated quantities,

$$P(E,t)=\int_{E-\Delta E/2}^{E+\Delta E/2} dE|a(E,t)|^2, \tag{22}$$

for the narrow discretized energy interval ΔE, and

$$P_{\text{cont}}(t)=\int_0^{E_{\max}} dE|a(E,t)|^2, \tag{23}$$

for the total population of all continuum states, which is equivalent to the dissociation probability $\mathscr{D}(t)$ of Eq. (12). The results obtained by the approximate IDE approach of Eq. (18) are treated in comparison with those obtained by the exact STP method.

In the design of optimal laser fields for controlling the molecular dynamics the use is made of a superposition of several laser pulses constituting the global laser field

$$\mathscr{E}(t)=\sum_k \mathscr{E}_k \sin^2[\pi(t-t_{0k})/t_{pk}]\cos[\omega_k(t-t_{0k})+\varphi_k], \tag{24}$$

where pulse k, which has duration t_{pk}, starts at $t=t_{0k}$, i.e., the current time interval is

$$t_{0k}\leqslant t\leqslant t_{0k}+t_{pk}, \tag{25}$$

$\mathscr{E}_k$ is the electric field amplitude of the kth pulse, ω_k is the respective laser carrier frequency, and φ_k is the phase.

The amplitudes $\mathscr{E}_k$ and the carrier frequencies ω_k of the individual pulses are optimized separately in order to achieve a prespecified target: maximize the population of the target bound state along with minimizing the dissociation probability, localize the population in a narrow energy domain of continuum, or maximize the dissociation probability. The optimization procedure is described in Refs. 17, 46, and 49. Finally, the optimal overlaps of the pulses can be used in order to diminish the overall duration of the laser control.

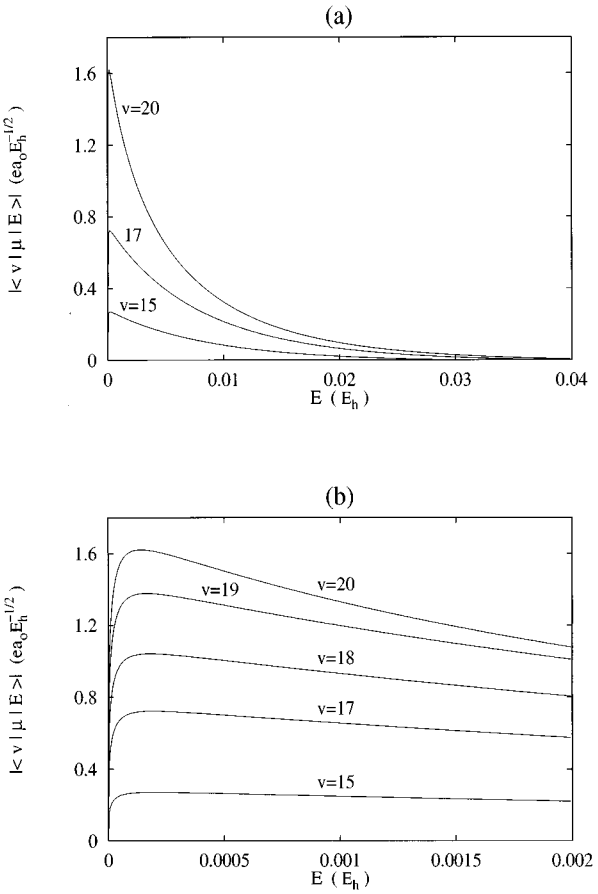

FIG. 1. Bound–continuum couplings for OH. Absolute values of the dipole moment matrix elements of the bound–continuum transitions are shown for two domains of the continuum energy (a) and (b). Numbers of the bound states are indicated near the curves.

The phases φ_k proved to be of minor importance in the developed laser control scheme, and all results below are demonstrated for $\varphi_k=0$. The pulse durations used in our simulations are 0.5 ps and 1 ps. The laser pulse shape of $\sin^2$ type is used in our simulations as in Refs. 15–17, for example. This shape is suitable, but rather arbitrary — very similar control schemes can be developed by means of other reasonable, ''bell'' type, shapes of the pulses, for example, Gaussians.

III. BOUND–CONTINUUM COUPLING AND SELECTIVE PREPARATION OF INTERMEDIATE BOUND STATES

Bound–continuum couplings, represented by the dipole moment matrix elements $\langle v|\mu|E\rangle$, provide important information about the bound states which are suitable for the state-selective preparation on the one hand, and for the subsequent excitation of the continuum states on the other hand. Figures 1(a) and 1(b) show the absolute values of some bound–continuum matrix elements for OH under investigation as functions of the continuum energy E for several high-lying bound states $|v\rangle$.

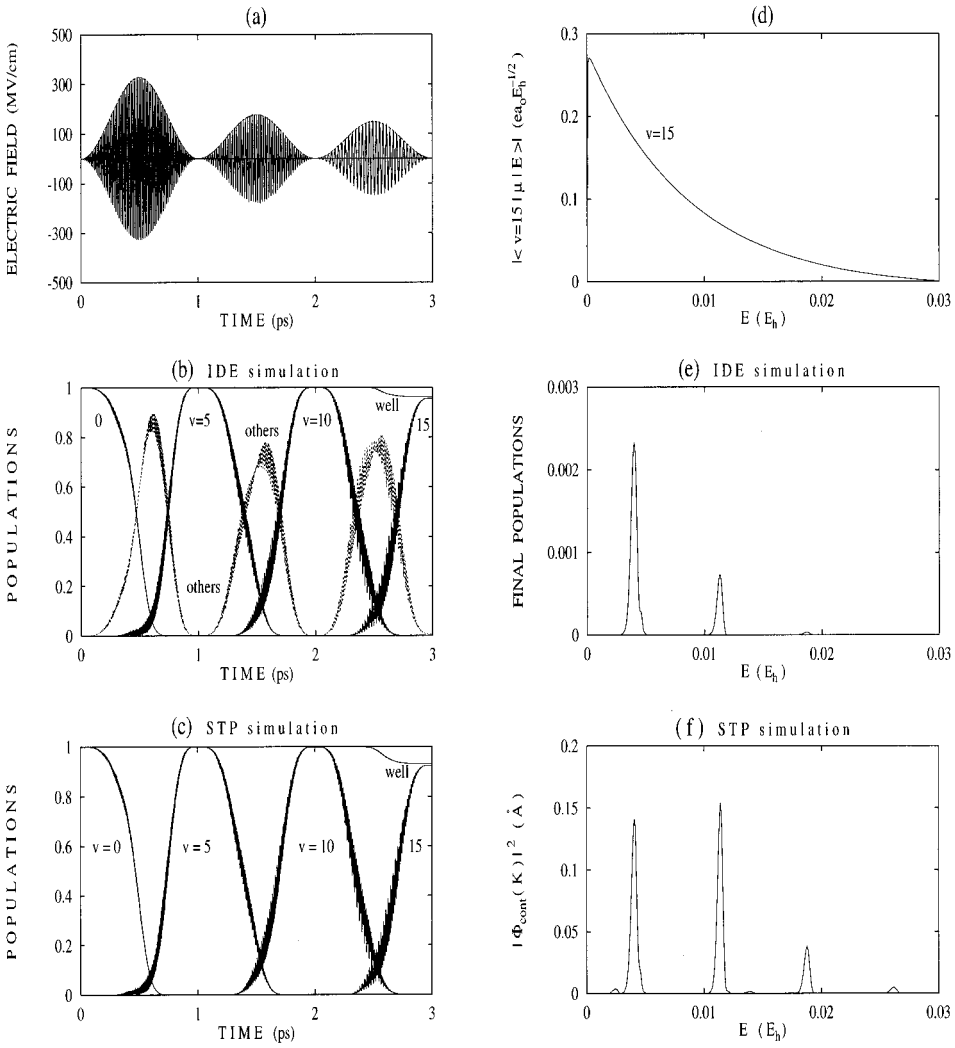

FIG. 2. State-selective preparation of OH in the bound state $|v=15\rangle$ by three non-overlapping 1 ps laser pulses, starting from $|v=0\rangle$. (a) Optimal laser field with the pulse parameters: $\mathscr{E}_1^{\rm opt}=328.05$ MV/cm, $\omega_1^{\rm opt}=3424.19$ cm^{-1}, $\mathscr{E}_2^{\rm opt}=176.44$ MV/cm, $\omega_2^{\rm opt}=2525.52$ cm^{-1}, $\mathscr{E}_3^{\rm opt}=148.07$ MV/cm, $\omega_3^{\rm opt}=1625.67$ cm^{-1}. (b) and (c) Population dynamics; numbers of levels are indicated near the curves, '' WELL'' — overall population of bound states. '' OTHERS'' — total population of bound states except those indicated explicitly, (d) Bound–continuum coupling for $|v=15\rangle$. (e) Final populations of the continuum states. (f) Continuum wave function in momentum space versus the energy.

The following features can be distinguished from Fig. 1: (i) the bound–continuum couplings increase with increasing number of the initial vibrational level v; (ii) the couplings first increase strongly with E, reaching their global maxima at $E<0.002$ D; and (iii) with further increasing energy E, they drastically decrease (at least by 1 order of magnitude at $E=0.1$ D and by 2 orders at $E=0.2$ D). These features make it possible to choose the discretized energy intervals $\Delta E_{(i)}$, and the upper limit $E_{\max}$ for the integration over the continuum energy E in the IDE (18).

As our target for the state-selective preparation we choose $|v=15\rangle$. This state is not very strongly coupled to continuum, as can be seen from Fig. 1, therefore it can be prepared state-selectively starting from the vibrational ground state, and serve as a suitable intermediate state for selective preparation of the very top states. At the same time, its coupling to the continuum states should not be neglected, which allows us to study the dissociation which accompanies the state-selective preparation. The state-selective preparation of $|v=15\rangle$ can be controlled by superposition of three laser pulses which pump successive 5-photon resonance transitions according to the excitation pathway

$$|0\rangle\rightarrow(5\text{ photons})\rightarrow|5\rangle\rightarrow(5\text{ photons})\rightarrow|10\rangle \rightarrow(5\text{ photons})\rightarrow|15\rangle \tag{26}$$

via the intermediate resonant states $|v=5\rangle$ and $|v=10\rangle$. The control laser field is optimized by using the sequential control scheme.[49] The optimal sequence of three non-overlapping laser pulses of 1 ps duration is shown in Fig. 2(a). The respective population dynamics simulated by the IDE and STP approaches is presented in Figs. 2(b) and 2(c), correspondingly. It is clearly seen from Figs. 2(b) and 2(c), that both intermediate states, $|v=5\rangle$ and $|v=10\rangle$, can be

prepared selectively with probability close to 100%. The laser-induced coupling to the continuum states becomes noticeable only for vibrational levels $v>10$.

The final population of the target state $|v=15\rangle$ at the end of the third laser pulse, resulting from the IDE simulations, is $P_{15}(t_{03}+t_{p3})=0.9557$ with the state-selectivity $\mathscr{S}_{15}(t_{03}+t_{p3})=0.9939$. The overall population of the continuum states $P_{\rm cont}(t_{03}+t_{p3})=0.0397$. The respective results of the STP simulations are: $P_{15}(t_{03}+t_{p3})=0.9241$, $\mathscr{S}_{15}(t_{03}+t_{p3})=0.9923$, and the dissociation probability is $\mathscr{D}(t_{03}+t_{p3})=0.0688$.

While the state-selectivities for preparation of OH in the target state $|v=15\rangle$ resulting from the IDE and STP simulations are in a very good agreement, the total population remaining in the well is smaller by about 3% for the STP approach. Though this difference is of minor importance for the bound states, it implies almost 40% difference for the dissociation probability, which indicates the influence of the continuum–continuum transitions, see also Ref. 68.

The population of the continuum states at the end of the three-pulse sequence, as it is simulated within the IDE approach, are shown in Fig. 2(e) for the evenly discretized energy intervals of $\Delta E=0.00005$ hartree. The continuum state populations are localized in three narrow energy domains separated by the energy interval of $\hbar\omega$, where ω is the laser carrier frequency optimized for the 5-photon transition $|10\rangle\rightarrow|15\rangle$. The first peak in the continuum is separated from the target level $v=15$ by the energy interval of $3\hbar\omega$. This indicates the laser-induced 3-photon, 4-photon and 5-photon transitions between the bound state $|15\rangle$ and the respective continuum states, keeping in mind that the continuum–continuum transitions are not taken into account in the IDE approach. The heights of the peaks reflect the strength of the laser-induced coupling between state $|v=15\rangle$ and the respective continuum states. The coupling is represented by the dipole moment matrix element $\langle v=15|\mu|E\rangle$, which is shown in Fig. 2(d). The bound–continuum coupling is noticeable for the continuum states in the vicinity of 3-photon and 4-photon resonances with the bound state $|v=15\rangle$, and it is very small for the 5-photon resonance. Therefore, for the laser frequencies used here there are only two efficient pathways for excitation of the continuum states from the bound state $|v=15\rangle$.

During the state-selective preparation of the bound state $|v=15\rangle$ the laser-induced continuum–continuum transitions are more important for the continuum states than for bound states. This is illustrated in Fig. 2(f) for the continuum wave function in momentum space at the end of the three-pulse pumping, $|\Phi_{\rm cont}(K,t_{03}+t_{p3})|^2$, which is plotted versus the energy $E=(\hbar K)^2/2m$. It is seen from Fig. 2(f) that the laser induced continuum–continuum transitions result in increasing the second peak in continuum in comparison with the first one and cause the fourth, comparatively small peak to appear. The last peak is not seen in the IDE picture, Fig. 2(e).

Dissociation spectra presented in Figs. 2(e) and 2(f) are typical for above-threshold dissociation (ATD),[69–73] — a nonlinear phenomenon in which a molecule absorbs more photons than the minimum number necessary for dissociation, and additional quanta of photon energy appear as evenly spaced peaks in the dissociation spectra.

Another possibility to prepare OH selectively in the bound state $|v=15\rangle$ is to pump in the third step of the control scheme the overtone transition $|10\rangle\rightarrow|15\rangle$. This yields the excitation pathway

$$|0\rangle\rightarrow(5\text{ photons})\rightarrow|5\rangle\rightarrow(5\text{ photons})\rightarrow|10\rangle \rightarrow(1\text{ photon})\rightarrow|15\rangle. \tag{27}$$

The overall time of the molecular state-selective preparation can be reduced by employing shorter and overlapping pulses. In the first two steps of the excitation pathway (27), the use is made of two 0.5 ps laser pulses with a 0.15 ps overlap. In the third step, a 1 ps pulse is used for pumping overtone transition with a 0.25 ps overlap with the second pulse. The amplitudes $\mathscr{E}_k$ and the carrier frequencies ω_k of the individual pulses, which constitute the global laser field, have been optimized separately in order to achieve maximal population of the target bound state $|v=15\rangle$, along with minimizing the dissociation probability. Finally, the overlaps of the pulses have been introduced in order to diminish the overall duration of the state-selective preparation without a noticeable decrease of the resulting state-selectivity for the level $v=15$, and without any additional optimization of the laser pulse amplitudes and carrier frequencies (which is also possible). The global laser field is shown in Fig. 3(a).

The respective population dynamics is shown in Figs. 3(b) and 3(c) for the IDE and STP simulations, correspondingly. The final population of the target state $|v=15\rangle$ at the end of the overlapping pulse sequence, as obtained by the IDE simulations, is $P_{15}(t_{03}+t_{p3})=0.9639$. The total population of the bound states is $P_{\rm well}(t_{03}+t_{p3})=0.9763$, implying the state-selectivity $\mathscr{S}_{15}(t_{03}+t_{p3})=0.9874$. The overall population of the continuum states $P_{\rm cont}(t_{03}+t_{p3})=0.0237$. The corresponding STP simulations yield for the bound states: $P_{\rm well}(t_{03}+t_{p3})=0.9586$, $P_{15}(t_{03}+t_{p3})=0.9454$, and the state-selectivity is $\mathscr{S}_{15}(t_{03}+t_{p3})=0.9862$, with the dissociation probability $\mathscr{D}(t_{03}+t_{p3})=0.0414$.

In the case of pumping the overtone transition $|v=10\rangle\rightarrow|v=15\rangle$ in the third step of the excitation pathway, the IDE simulations for the continuum states are in better agreement with the exact STP simulations, than in the case of pumping the respective 5-photon transition. This concerns both the bound states and the continuum states.

The continuum states populations are localized in a single and narrow energy domain. This is shown in Fig. 3(e) for the IDE simulated results with the discretized energy intervals $\Delta E=0.0001$ hartree, and in Fig. 3(f) for the STP generated continuum wave function in momentum space at the end of the three-pulse pumping, which is plotted versus the energy E. The target bound state $|v=15\rangle$ and the selectively populated domain of the continuum are spaced by the energy interval of $\hbar\omega$, where ω is the laser carrier frequency optimized for the overtone transition $|10\rangle\rightarrow|15\rangle$.

The reason for formation of a single peak in continuum is evident from Fig. 3(d), where the dipole moment matrix element $\langle v=15|\mu|E\rangle$ is also plotted against the energy E.

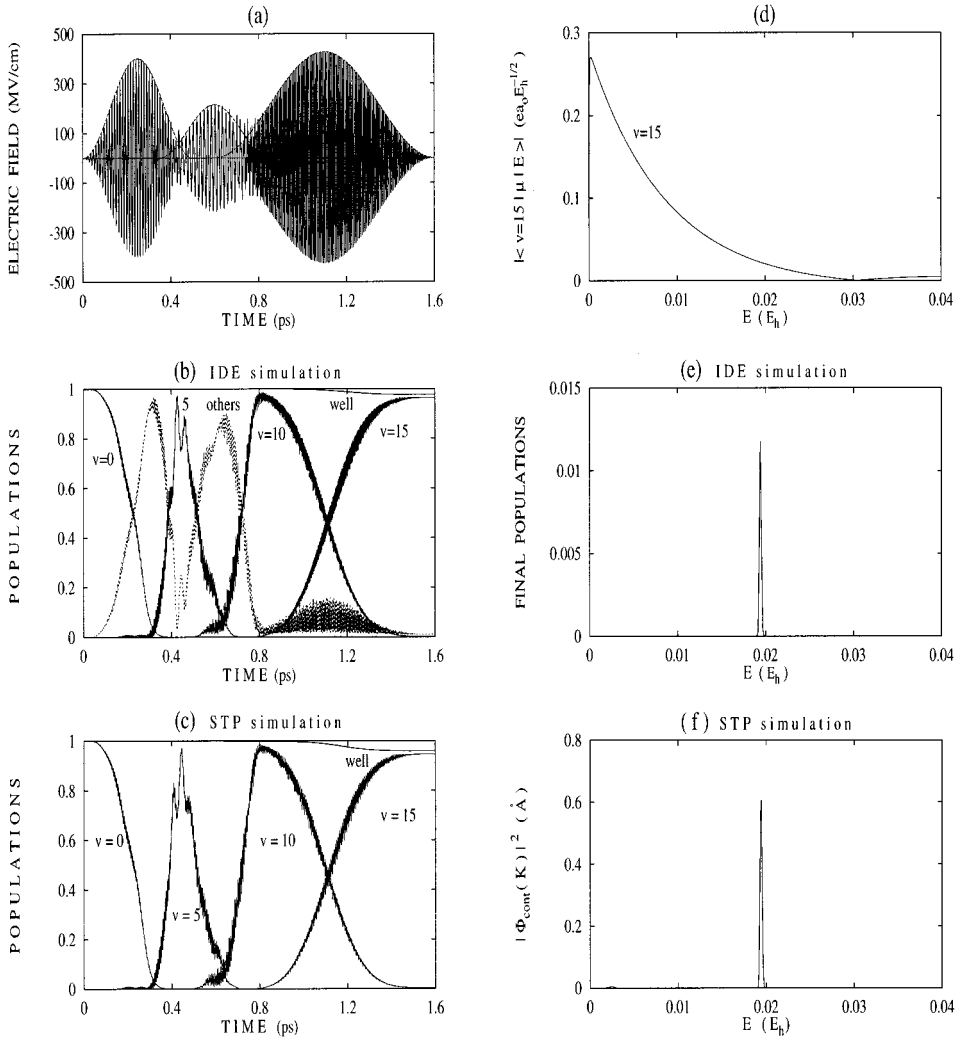

FIG. 3. State-selective preparation of OH in the bound state $|v=15\rangle$ by three overlapping laser pulses, starting from $|v=0\rangle$. (a) Optimal laser field with the pulse parameters: $\mathscr{E}_1^{\rm opt}=400.75$ MV/cm, $\omega_1^{\rm opt}=3425.79$ cm^{-1}, $t_{p1}=0.5$ ps, $\mathscr{E}_2^{\rm opt}=214.56$ MV/cm, $\omega_2^{\rm opt}=2524.69$ cm^{-1}, $t_{p2}=0.5$ ps, $t_{02}=0.35$ ps, $\mathscr{E}_3^{\rm opt}=426.47$ MV/cm, $\omega_3^{\rm opt}=8148.58$ cm^{-1} $t_{p3}=1$ ps, $t_{03}=0.6$ ps. (b) and (c) Population dynamics; labelling is as in Figs. 2(b) and 2(c). (d) Bound–continuum coupling for $|v=15\rangle$. (e) Final populations of the continuum states. (f) Continuum wave function in momentum space versus the energy.

The bound–continuum coupling is noticeable only for the continuum states in the vicinity of 1-photon resonance with the bound state $|v=15\rangle$, and it is very small for the 2-photon resonance. Therefore, for the laser frequencies used here there is only one efficient pathway for exciting the continuum states from the bound state $|v=15\rangle$. The fact, that additional peaks do not appear in the STP picture of the dissociation spectrum, Fig. 3(f), implies weak continuum–continuum couplings between the respective continuum states.

The dissociation probability in the case of pumping in the last stage the overtone transition $|10\rangle\rightarrow|15\rangle$ is about two times smaller than the dissociation probability for the respective 5-photon transition. This allows one to assume that large photon energy and a few efficient excitation pathways into the continuum associated with the overtone excitation are more suitable for state-selective preparation of a molecule in high-lying bound states, close to dissociation threshold, while comparatively small photon energy corresponding to the multiphoton excitation and several excitation pathways into continuum may result in efficient dissociation.

IV. ABOVE-THRESHOLD AND STATE-SELECTIVE DISSOCIATION

In this section we assume that OH is already prepared selectively in the bound vibrational state $|v=15\rangle$ by using the technique described above and consider its dissociation starting from $|v=15\rangle$ as initial state. We investigate two approaches for dissociation: (i) direct 1-photon excitation of continuum states, and (ii) multiphoton excitation via a higher-lying bound state. The former approach implies making use of more intense laser fields for dissociation on a fs/ps time scale because the bound–continuum coupling for state $|v=15\rangle$ is not very strong (see Fig. 1), but it can yield controllable state-selectivity for continuum excitation. On the other hand, multiphoton excitation via a higher bound state should profit from its strong bound–continuum coupling and

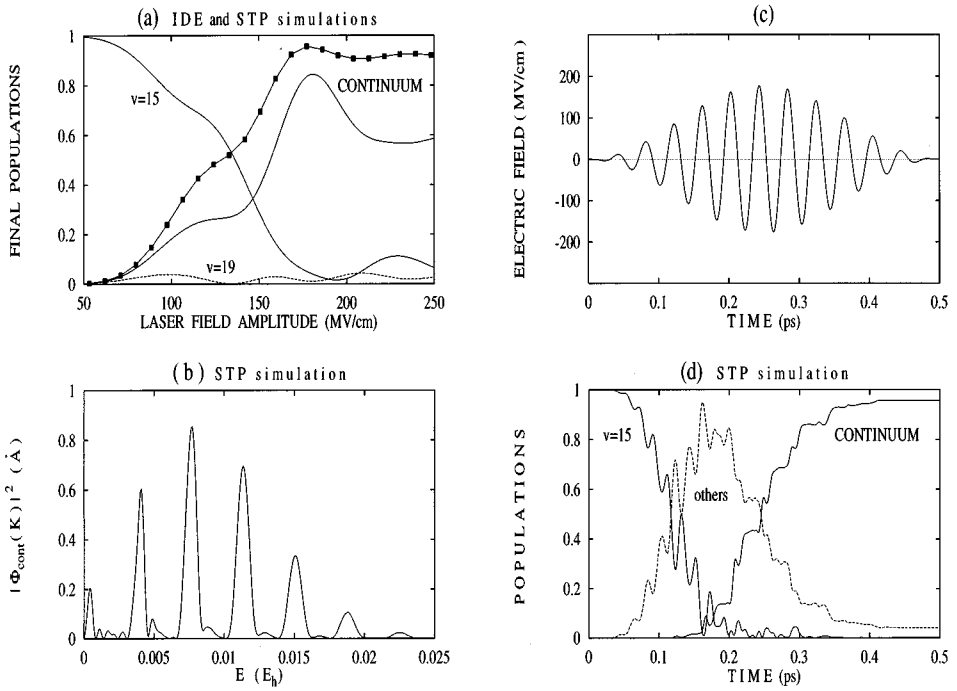

FIG. 4. Multiphoton above-threshold dissociation of OH from the bound state $|v=15\rangle$. Numbers of the bound states are indicated near the curves, ''CONTINUUM'' – total population of the continuum states. (a) Optimization of the laser pulse amplitude at the laser carrier frequency $\omega_1=822.448\ \mathrm{cm}^{-1}$ and $t_{p1}=0.5$ ps. (b) Continuum wave function in momentum space versus the energy. (c) Optimal laser pulse: $\mathscr{E}_1^{\mathrm{opt}}=177.32$ MV/cm, $\omega_1^{\mathrm{opt}}=822.448\ \mathrm{cm}^{-1}$ at $t_{p1}=0.5$ ps. (d) Population dynamics.

from several efficient excitation pathways into continuum as well, which yields less state-controllable but more efficient dissociation.

Starting with the multiphoton dissociation from $|v=15\rangle$, we choose $|v=19\rangle$ as a higher intermediate bound state which, being pumped in 4-photon resonance, is spaced by one quantum of photon energy from the continuum states lying in the vicinity of maximal bound–continuum coupling represented by the matrix element $\langle v=19|\mu|E\rangle$ (see Fig. 1). This also implies several efficient multiphoton transitions into the continuum, which are enhanced by the continuum-continuum transitions. The supposingly dominant excitation pathway can be presented schematically as follows:

$$|v=15\rangle\rightarrow(4\ \text{photons})\rightarrow|v=19\rangle\rightarrow(1\ \text{photon})\rightarrow\{|E_{(1)}\rangle\}\rightarrow(1\ \text{photon})\rightarrow\{|E_{(2)}\rangle\}\rightarrow\ldots, \quad (28)$$

where $\{|E_{(k)}\rangle\}$, $k=1,2,\ldots$, stand for continuum states close to resonance with the laser field, which are usually represented by sequential peaks in the dissociation spectra. This excitation pathway is to be realized by a single pulse pumping, and in the following it is shown that it can yield above-threshold dissociation.

As soon as the laser carrier frequency is fixed by the exact resonance for 4-photon transition $|15\rangle\rightarrow|19\rangle$, only the laser field strength should be optimized. Figure 4(a) shows final populations at the end of the 0.5 ps laser pulse as functions of its electric field amplitude resulted from both IDE simulations (lines) and STP simulations (dark points joined with lines). Curve ''CONTINUUM'' gives overall population of continuum states or dissociation probability. The IDE simulations give the correct optimal laser field strength, while the dissociation probability is smaller by about 10% as compared to the STP approach which yields maximal dissociation probability $\mathscr{D}=0.9564$ at $\mathscr{E}^{\mathrm{opt}}=177.32$ MV/cm. The optimal laser pulse is shown in Fig. 4(c), and the respective population dynamics is presented in the bottom, Fig. 4(d), where curve ''others'' gives total population of all bound states except $|v=15\rangle$, which is presented by the separate curve. The dissociation spectrum presented in Fig. 4(b) is the signature of the ATD spectrum, with the spacing between the peaks being equal to one quantum of photon energy. At the same time, the sequential peaks in Fig. 4(b) are not separated from the resonant bound state $|v=19\rangle$ by any integer numbers of photons, but they are shifted to slightly smaller energies. This reflects the influence of other, non-resonant bound states, mostly $16<v<19$, which acquire substantial populations during the excitation process, as seen from Fig. 4(d). The dissociation described above will be referred to as multiphoton ATD.

The multiphoton excitation of OH prepared selectively in a certain bound vibrational state, which results in multiphoton ATD, enables one to produce free H atoms with different, well established and well separated kinetic energies. In an optimal case, the dissociation probability may exceed $\mathscr{D}=0.96$ even in moderate laser fields, but the tools of control over the multiphoton ATD spectra are restricted to the choice of the initial bound state and the multiphoton resonance to be pumped. Detuning the laser carrier frequency off

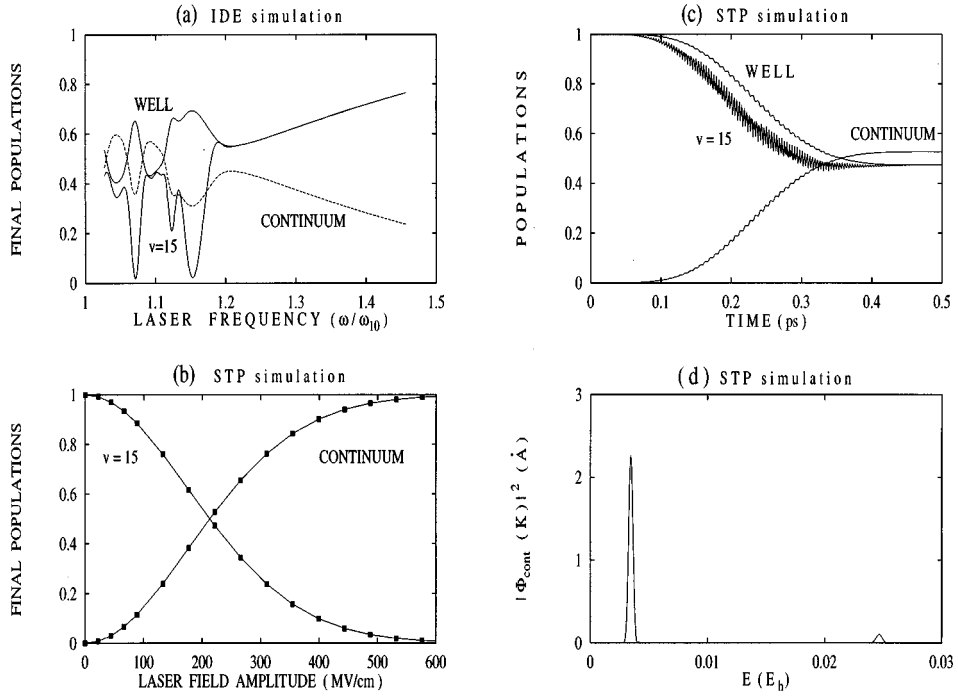

FIG. 5. One-photon dissociation of OH from the bound state $|v=15>$. Curve ''WELL'' gives the total population of the bound states, ''CONTINUUM'' – total population of the continuum states, the population of the initial state $|v=15\rangle$ is indicated explicitly. (a) Optimization of the laser carrier frequency at the laser pulse amplitude $\mathscr{E}_1=265.99$ MV/cm and $t_{p1}=0.5$ ps. (b) Optimization of the laser pulse amplitude at the laser carrier frequency $\omega_1=4654.60$ cm^{-1} and $t_{p1}=0.5$ ps. (c) Population dynamics at the optimal frequency $\omega_1^{\rm opt}=4654.60$ cm^{-1}, and $\mathscr{E}_1=221.66$ MV/cm, $t_{p1}=0.5$ ps. (d) Continuum wave function in momentum space versus the energy.

the resonance, in order to shift all the multiphoton ATD peaks for example, decreases the dissociation probability. The envelope of the multiphoton ATD spectrum, the number and the heights of the peaks as well as their positions, are not easily controlled. However, it is most desirable to obtain, for example, a single dominant peak in the continuum with controllable position in energy space, or several peaks with arbitrary positions.

More flexible tools of control over the dissociation spectra can be gained from direct 1-photon excitation of the continuum states. Starting from the selectively prepared bound state $|v=15\rangle$, the supposedly dominant excitation pathway can be presented schematically as follows:

$$|v=15\rangle\rightarrow(1\text{ photon})\rightarrow\{|E_{(1)}\rangle\}\rightarrow(1\text{ photon})\rightarrow\ \ldots\ . \tag{29}$$

This excitation pathway may require more intense laser fields than the multiphoton ATD, because of not very strong bound–continuum coupling for $|v=15\rangle$. On the other hand, the optimal laser carrier frequency can be varied in rather wide domain with two ''boundary'' restrictions: (i) decreasing of the bound–continuum coupling for high frequencies (see Fig. 1), which can be compensated by using stronger laser fields, and (ii) competition of the laser induced bound–bound transitions for low frequencies. Therefore, the first step in the optimization procedure should be optimization of the laser carrier frequency.

Figure 5(a) shows final populations at the end of the 0.5 ps laser pulse as functions of the laser carrier frequency at the laser field amplitude fixed to $\mathscr{E}_1=265.99$ MV/cm. Results are obtained from the IDE simulations. Sharp minima in the population of the initial state $|v=15\rangle$ at low frequencies result from the competition of the following bound-bound transitions:

$$\begin{aligned}&|15\rangle\rightarrow(1\text{ photon})\rightarrow|21\rangle,\quad |15\rangle\rightarrow(2\text{ photons})\rightarrow|10\rangle,\\ &|15\rangle\rightarrow(3\text{ photons})\rightarrow|9\rangle,\quad |15\rangle\rightarrow(1\text{ photon})\rightarrow|12\rangle,\end{aligned} \tag{30}$$

which are close to the respective resonances. This frequency domain is not suitable for the laser-induced dissociation. A promising domain is that of $\omega>1.2\omega_{10}$, where only the initial bound state $|v=15\rangle$ and continuum states are populated at the end of the laser pulse. Other bound states are not populated by the end of the pulse, which is very suitable for sequential pulse excitation. Therefore, it is reasonable to optimize the laser field amplitude for the carrier frequencies belonging to the aforementioned state-selective domain $\omega>1.2\omega_{10}$. Figure 5(b) shows the final populations at the end of the 0.5 ps laser pulse as functions of the electric field amplitude at the carrier frequency fixed to $\omega=1.23\omega_{10}$, resulting from the STP simulations (dark points joined with lines). Monotonous increase of the dissociation probability, represented by curve '' CONTINUUM,'' implies almost 100% dissociation in strong laser fields. It is also clear that complete dissociation from selectively prepared higher bound states, $v>15$, with stronger bound–continuum couplings (see Fig. 1) will require much weaker laser fields, than in the case of $|v=15\rangle$ under consideration. The problem of state-

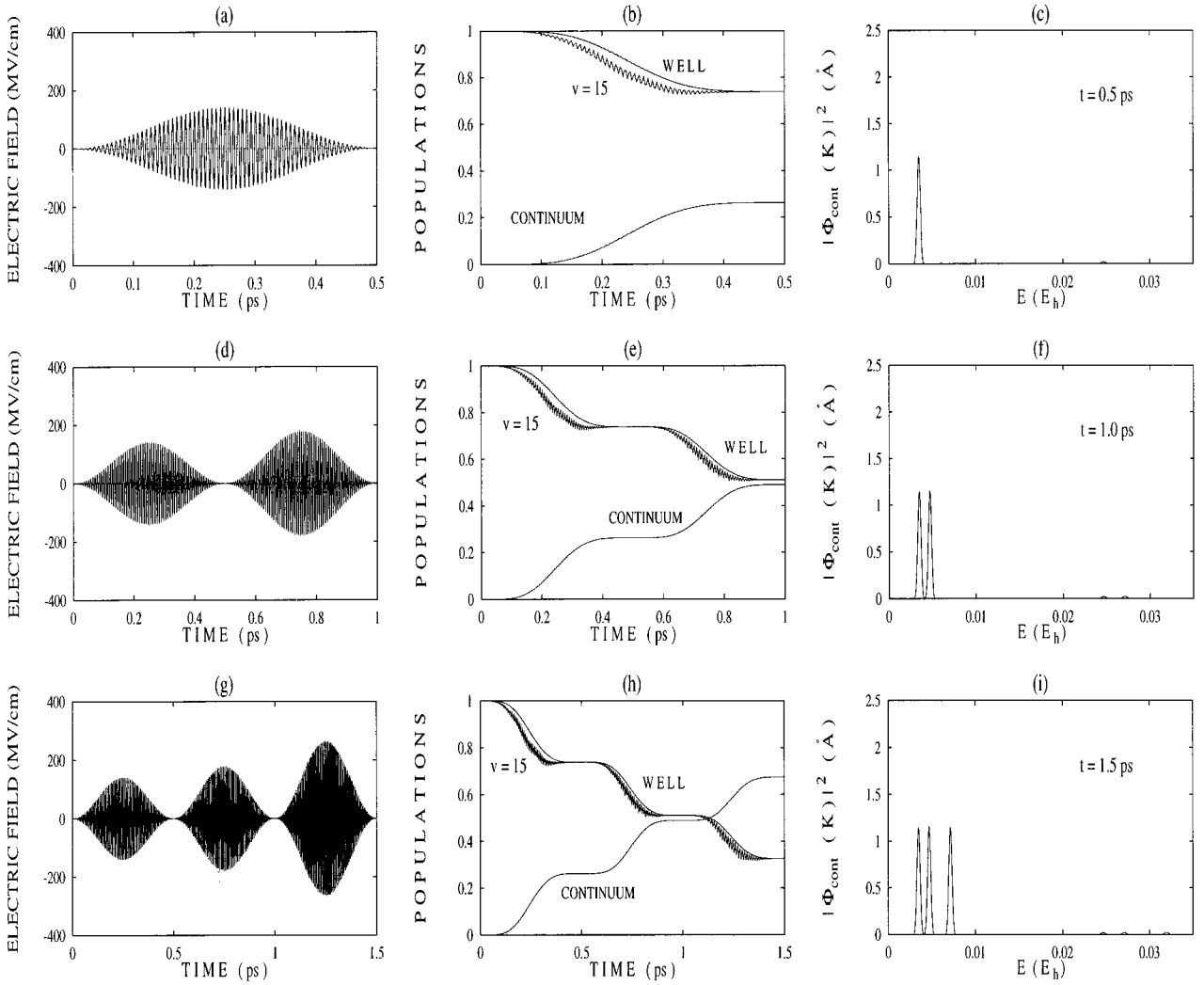

FIG. 6. State-selective control of the dissociation spectrum for OH under the successive excitation by 0.5 ps laser pulses from $|v=15\rangle$. Labelling is as in Fig. 5. Left-hand column (a), (d), and (g) — optimal laser pulses; middle column (b), (e), and (h) — population dynamics; right-hand column (c), (f), and (i) — dissociation spectra. Optimal pulse parameters: (a) $\mathscr{E}_1^{\rm opt}=140.09$ MV/cm, $\omega_1^{\rm opt}=4654.60$ cm^{-1}. (d) $\mathscr{E}_1^{\rm opt}$, $\omega_1^{\rm opt}$ are as in the case (a), and $\mathscr{E}_2^{\rm opt}=177.33$ MV/cm, $\omega_2^{\rm opt}=4919.50$ cm^{-1}. (g) $\mathscr{E}_1^{\rm opt}$, $\omega_1^{\rm opt}$, $\mathscr{E}_2^{\rm opt}$, $\omega_2^{\rm opt}$ are as in the case (d), and $\mathscr{E}_3^{\rm opt}=262.44$ MV/cm, $\omega_3^{\rm opt}=5449.29$ cm^{-1}.

selective preparation of top bound states is to be addressed in the next section. Here we consider laser-controllable selective excitation of continuum states. Figure 5(c) shows the population dynamics for a direct 1-photon excitation of the continuum states from the bound state $|v=15\rangle$ with a single 0.5 ps laser pulse. The respective dissociation spectrum is shown in Fig. 5(d). It represents a single dominant peak in continuum; its maximum is located in the vicinity of the resonant energy

$$E_{(1)}=E_{v=15}+\hbar\omega \tag{31}$$

with much better than 1% accuracy, on the contrary to the multiphoton ATD spectrum [Fig. 4(b)] which is shifted to smaller energies. The height of the dominant peak and its position in energy space are controllable: The height is controlled by the laser field amplitude, while the position is controlled by the laser carrier frequency, see Figs. 5(a) and 5(b). The second-order peak has a very small height, and it is separated from the first, strongly dominant peak by one quantum of photon energy. Therefore, the dissociation spectrum presented in Fig. 5(d) is also an ATD spectrum, but a very special one – with a single dominant peak, which is the signature of a 1-photon ATD for OH under study. The dissociation probability achieved with the laser pulse parameters $\mathscr{E}_1=221.66$ MV/cm and $\omega_1=4654.60$ cm^{-1} is $\mathscr{D}(t_p)=0.5268$, and the state-selectivity achieved by the end of the pulse with respect to the initial state is $\mathscr{S}_{15}(t_p)=0.9998$.

The fact that after a 1-photon dissociation from a selectively prepared bound state all non-dissociating molecules may return to the initial bound state with almost 100% probability enables one to achieve a flexible state-selective control of the dissociation spectra by making use of sequential laser pulses with different carrier frequencies and amplitudes. Figure 6 gives three examples of 1-photon dissocia-

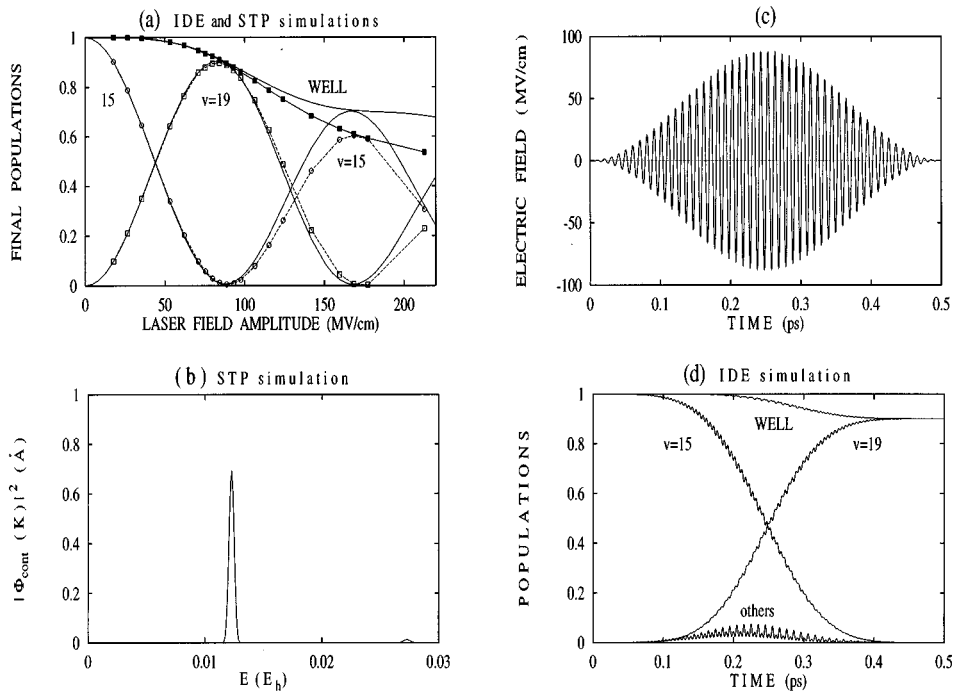

FIG. 7. State-selective preparation of OH in the bound state $|v=19\rangle$ by the overtone transition from $|v=15\rangle$. Numbers of the bound states are indicated near the curves, ''WELL'' – overall population of the bound states. (a) Optimization of the laser pulse amplitude at the laser carrier frequency $\omega_1=3289.78$ cm^{-1} and $t_{p1}=0.5$ ps. (b) Continuum wave function in momentum space versus the energy. (c) Optimal laser pulse: $\mathscr{E}_1^{opt}=87.776$ MV/cm, $\omega_1^{opt}=3294.32$ cm^{-1} at $t_{p1}=0.5$ ps. (d) Population dynamics.

tions by one [Figs. 6(a)–6(c)] two [Figs. 6(d)–6(f)], and three [Figs. 6(g)–6(i)] laser pulses of 0.5 ps duration with the laser carrier frequencies increasing from pulse to pulse. Driving laser pulses are shown in the left-hand column of Fig. 6, the respective population dynamics — in the middle column, and dissociation spectra — in the right-hand column, correspondingly. It is clearly seen that one-pulse dissociation yields one strongly dominant peak in the dissociation spectrum, two-pulse dissociation yields two strongly dominant peaks while three-pulse dissociation yields three dominant peaks. The carrier frequency of the second laser pulse is chosen to yield the second peak very close to the first one, and the frequency of the third laser pulse is chosen to yield the third peak apart from the first two. The amplitudes of the pulses are specially chosen to yield equal heights of the dominant peaks in the dissociation spectra, emphasising the flexibility of control. The higher-order peaks generated by each of the laser pulses have very small heights, and they are of minor importance.

Contrary to the multiphoton ATD spectra, positions, heights, and times of appearance of dominant peaks in the 1-photon dissociation with sequential laser pulses are controllable by frequency, amplitude and time-delay of the pulses, correspondingly. This implies time-selective and space-selective control of the dissociation fragments. For OH under study one can envisage an experiment in which OH is adsorbed on a surface with a high adsorption energy, for example OH on Ni(111)[74] where strong coupling to the surface diminishes the role of rotation and orientation and may allow dissociation to be realized without substantial desorption on the one hand, and yield unidirectional beams of the H atoms on the other hand. For example, in the case of sequential three-pulse 1-photon dissociation [Figs. 6(g)–6(i)], parameters of the laser pulses can be chosen enabling three wave packets representing free H atoms to be superimposed in a prescribed space-domain at a prescribed time to form a sort of a transition state suitable for collisions, or for chemical reactions with other reactants.

To conclude this section, both 1-photon and multiphoton dissociation from a selectively prepared bound state $|v=15\rangle$ can be joined to the stage of preparation, see Figs. 2 and 3, to yield the dissociation from the vibrational ground state. The influence of the preparation stage is of minor importance for dissociation because of very small dissociation probability during the preparation of $|v=15\rangle$. The respective laser control scheme may include four or more sequential, or overlapping laser pulses.

V. ULTRAFAST SELECTIVE PREPARATION OF TOP VIBRATIONAL BOUND STATES

It is well known that multiphoton excitation of molecules may change radically the dynamics of molecular and atom–molecular collisions. Of special interest is ultrafast selective preparation of high-lying vibrational eigenstates which can yield a stable molecule with large collisional cross-section. Besides the collision dynamics, selective preparation of high-lying bound states, close to the dissocia-

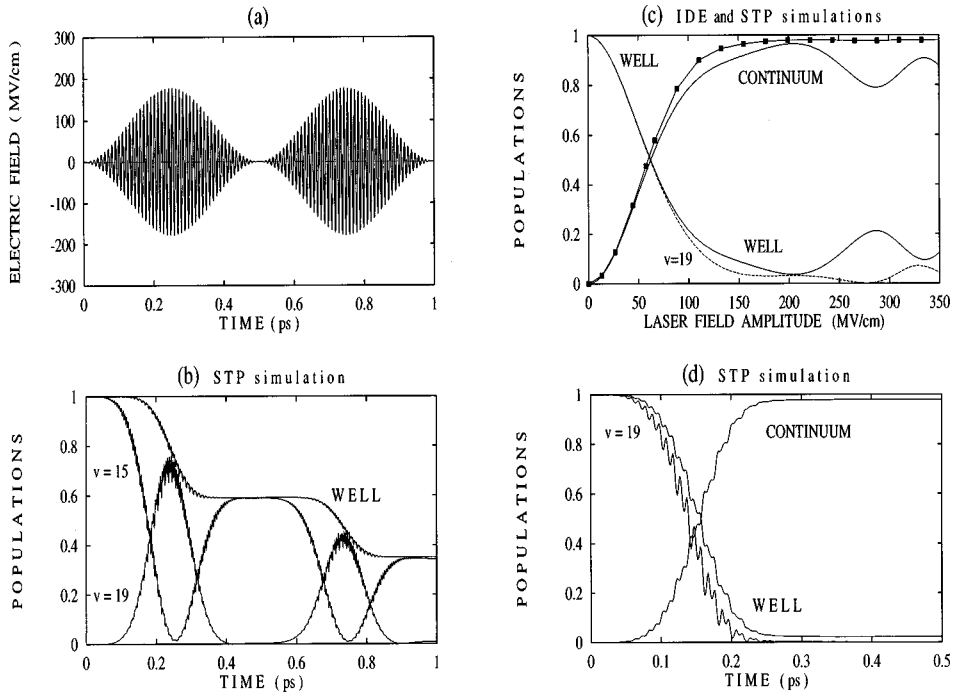

FIG. 8. Dissociation of OH by 0.5 ps laser pulses from the bound state $|v=15\rangle$ (a) and (b), and from $|v=19\rangle$ (c) and (d). Numbers of the bound states are indicated near the curves, ''WELL'' – overall population of the bound states. ''CONTINUUM'' – overall population of the continuum states. (a) Optimal two-pulse sequence for initial state $|v=15\rangle$. (b) Population dynamics at the optimal pulse parameters $\mathscr{E}_1^{\rm opt}=\mathscr{E}_2^{\rm opt}=177.33$ MV/cm, $\omega_1^{\rm opt}=\omega_2^{\rm opt}=3289.78$ cm^{-1}. (c) Optimization of the laser pulse amplitude for initial state $|v=19\rangle$ at the laser carrier frequency $\omega_1=1692.35$ cm^{-1} and $t_p=0.5$ ps. (d) Population dynamics at the optimal pulse parameters $\mathscr{E}_1^{\rm opt}=199.49$ MV/cm, $\omega_1^{\rm opt}=1692.35$ cm^{-1}.

tion threshold, is important for stimulating chemical reactions, laser-induced and collision-induced dissociation and spectroscopic studies as well.

In this section we investigate the process of ultrafast selective preparation of very high-lying bound vibrational states of OH including the very top state $|v=21\rangle$. Our main goal is to achieve maximal, close to 100%, state-selectivity of molecular preparation along with minimizing the dissociation probability. At the same time, several possibilities for efficient dissociation are also investigated. As in the previous section, we assume OH to be already prepared selectively in the intermediate bound state $|v=15\rangle$. To demonstrate the specific of state-selective preparation we first choose bound state $|v=19\rangle$ as a target. It has been shown in the previous section (see Fig. 4) that the 4-photon resonance pumping of $|15\rangle\rightarrow|19\rangle$ transition can yield a very efficient dissociation, but it is not suitable for state-selective preparation. In contrast, it is shown below that the overtone pumping with the respective excitation pathway

$$|v=15\rangle\rightarrow(1\ \text{photon})\rightarrow|v=19\rangle \tag{32}$$

can yield a very high state-selectivity along with a small dissociation probability, if the driving laser pulse is properly optimized.

Figure 7(a) illustrates the first step of the optimization procedure – optimization of the laser field amplitude. Final populations at the end of the 0.5 ps laser pulse which pumps the overtone transition $|15\rangle\rightarrow|19\rangle$ are shown therein as functions of its electric field amplitude resulting from both IDE simulations (lines) and STP simulations (points joined with lines). The laser carrier frequency is fixed to the exact 1-photon resonance. The results of IDE simulations are in a very good agreement with the exact STP results up to the electric field strength $\mathscr{E}_1\approx100$ MV/cm, yielding the first maximum of the state-selectivity at $\mathscr{E}_1^{\rm opt}=87.776$ MV/cm. A minor additional optimization of the laser carrier frequency yields the final state-selectivity $\mathscr{S}_{19}(t=t_p)=0.9999$. The optimal laser pulse is shown in Fig. 7(c), and the respective population dynamics is presented in the bottom, Fig. 7(d). The dissociation spectrum presented in Fig. 7(b) is a typical 1-photon ATD spectra with a strongly dominant first-order peak and a small second-order peak spaced from the first one by one quantum of photon energy. The dissociation probability at the end of the optimal laser pulse is $\mathscr{D}(t=t_p)=0.0999$.

It is also seen from the optimization curves presented in Fig. 7(a) that at a certain laser field strength, specifically at $\mathscr{E}_1=177.32$ MV/cm, the dissociation probability $\mathscr{D}(t=t_p)\approx0.4$, and non-dissociating molecules return back to the initial bound state $|v=15\rangle$ with almost 100% probability. This fact can be used to enhance dissociation by pumping the overtone transition $|15\rangle\rightarrow|19\rangle$ with sequential laser pulses. As an example, we illustrate in Figs. 8(a) and 8(b) the process of two-pulse dissociation with 0.5 ps laser pulses. The optimal two-pulse sequence is shown in Fig. 8(a), and the respective population dynamics — in Fig. 8(b). The overall time of the multiple-pulse dissociation can be diminished

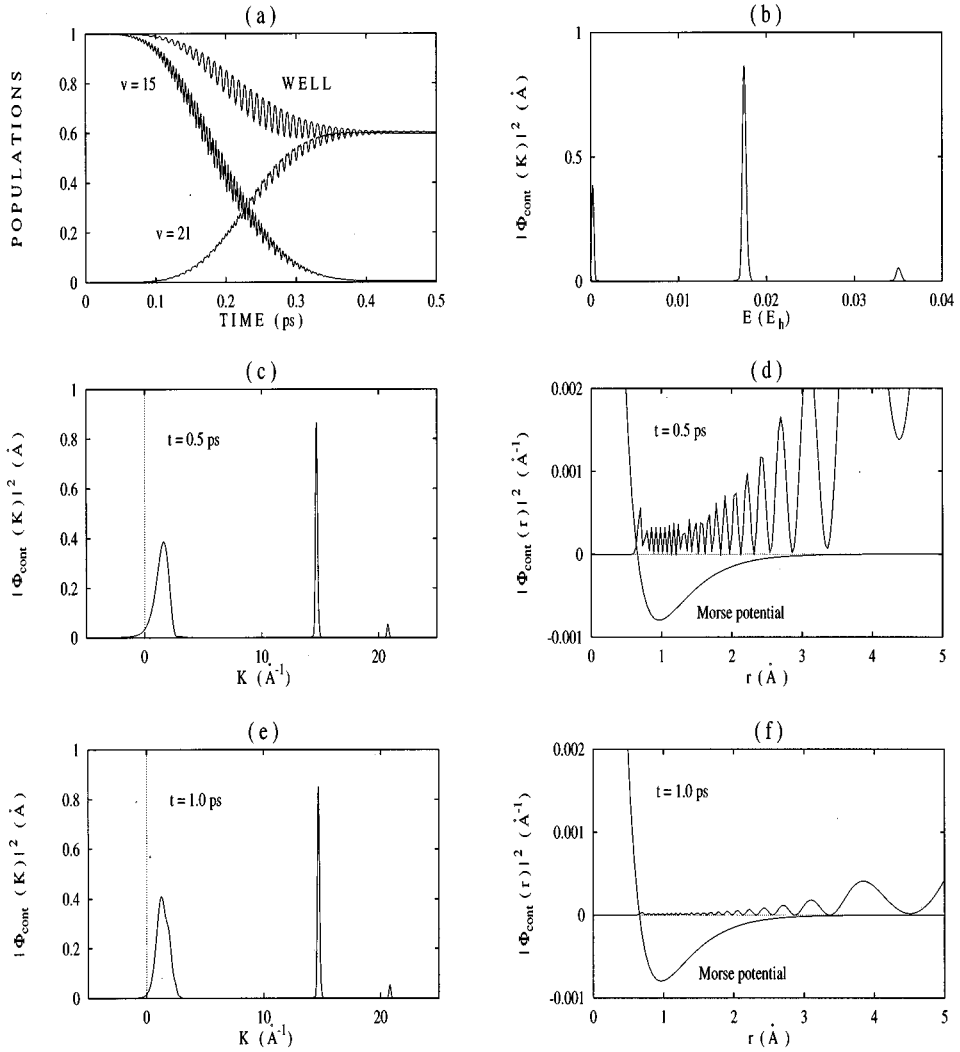

FIG. 9. State-selective preparation of OH in the highest bound state $|v=21\rangle$ by the overtone transition from $|v=15\rangle$. Numbers of the bound states are indicated near the curves, ''WELL'' – overall population of the bound states. (a) Population dynamics at the optimal pulse parameters $\mathscr{E}_1^{\rm opt}=267.39$ MV/cm, $\omega_1^{\rm opt}=3857.64$ cm^{-1}, and $t_{p1}=0.5$ ps. (b) Dissociation spectrum by the end of the pulse. Continuum wave function in momentum space (c) and in configuration space (d) by the end of the pulse. Continuum wave function in momentum space (e) and in configuration space (f) after a 0.5 ps free evolution since the end of the pulse.

by making use of shorter and overlapping laser pulses.

Another possibility to achieve an efficient dissociation is direct 1-photon excitation of the continuum starting from the selectively prepared high-lying bound state $|v=19\rangle$. Fig. 8(c) shows the final populations at the end of the 0.5 ps laser pulse as functions of its electric field amplitude resulted from STP simulations (points joined with lines) and IDE simulations (lines). The laser carrier frequency is fixed to $\omega=1692.35$ cm^{-1}, which is not far off the optimal value corresponding to the maximal bound–continuum coupling for $|v=19\rangle$ (see Fig. 1). The dissociation probability by the end of the pulse is $\mathscr{D}(t=t_p)>0.96$ at a field strength $\mathscr{E}(t=t_p)>155$ MV/cm. Population dynamics is presented in Fig. 8(d). It is seen from Fig. 8(d) that the laser pulse duration could be chosen about two times shorter, and it can yield almost the same dissociation probability. Additional optimization of the laser carrier frequency with respect to the state-selectivity of $|v=19\rangle$, similar to that demonstrated in the previous section for $|v=15\rangle$ (see Fig. 5), will result in similar tools of flexible control of the dissociation spectra (see Fig. 6), implying similar time-selective and space-selective control of the fragments, but much less demanding for the laser field strength.

State-selective preparation of the very top bound state $|v=21\rangle$ is achieved by making use of an optimization procedure similar to that demonstrated for $|v=19\rangle$. The excitation pathway is

$$|v=15\rangle\rightarrow(1\ \text{photon})\rightarrow|v=21\rangle. \tag{33}$$

In Fig. 9(a) we show the population dynamics stimulated by the optimal laser pulse of 0.5 ps duration which is preparing the target bound state $|v=21\rangle$ with the final population $P_{21}(t=t_p)=0.5969$ and the state-slectivity $\mathscr{S}_{21}(t=t_p)=0.9890$, starting from $|v=15\rangle$ as the initial state. The dissociation probability by the end of the pulse is

$\mathcal{D}(t=t_p)=0.3963$, which is at least four times larger than for any other high-lying bound state, including $|v=19\rangle$ and $|v=20\rangle$.

Another specific feature of the very top state preparation, Fig. 9(b), is the appearance of an additional, strong peak in the dissociation spectrum at a very small energy including $E=0$. This peak is referred to here as a zero-order one, because its position in energy space corresponds to less than the minimum number of photons necessary for dissociation from the initial state $|v=15\rangle$ when pumping a 1-photon transition $|15\rangle \rightarrow |21\rangle$. The other two peaks are the familiar first-order peak and the very small second-order peak. The three peaks are spaced by one quantum of photon energy, which is the signature of the ATD spectrum, but it includes a new component — the zero-order peak. The overall ATD spectrum presented in Fig. 9(b) is shifted to higher energy off the resonance with respect to bound states $|v=15\rangle$ and $|v=21\rangle$, in contrast to the multiphoton ATD spectrum described in the previous section [see Fig. 4(b)] which is shifted to smaller energies.

The continuum wave function by the end of the laser pulse, which is depicted in Fig. 9(c) in momentum space, clarifies that the momenta of fragments have noticeable negative and equal to zero components. This implies the appearance of dissociation fragments, specifically H atoms, with very small and even zero kinetic energy in analogy to electrons with zero kinetic energy in ZEKE spectroscopy.[75]

The continuum wave function in configuration space by the end of the laser pulse represents two well-localized wave packets corresponding to the dominant first-order peak and to the zero-order peak in the ATD spectrum. The wave packet corresponding to the zero-order peak also contains a sort of a standing wave just under the potential well, which is shown in Fig. 9(d). This standing wave indicates the formation of an overexcited quasi-bound molecular state, which resembles in part a bound state because a noticeable part of its wave function is located under the potential well, but it definitely belongs to the continuum states, because its average energy is $E>0$, though it is very small. The appearance of such states during the laser pulse excitation is readily understandable within the dressed states treatment, for example. Their existence after the end of the laser pulse is not trivial and may be useful for generating molecular transition states suitable for chemical reactions and collision processes as well. The continuum wave functions in momentum space and in configuration space after a 0.5 ps free evolution since the end of the laser pulse are presented in Figs. 9(e) and 9(f), respectively, and they show that the aforementioned quasi-bound molecular state exists at least on a fs time scale, which is known[76] to be long enough for the primary processes of chemical reactions, for example.

Selective preparation of quasi-bound molecular states of the type described above may prove to be very promising for many important fundamental applications, and it requires special investigation. Here we only indicate the possibility to prepare such states. Of special interest is the problem of selective preparation of long-living quasi-bound molecular states with the average energy very close to zero, implying preparation of a stable molecule ready for various transformations. As a good approximation to such state one may consider a molecule which has been selectively prepared in the very top vibrational bound state, as demonstrated in this section for preparation of OH in the very top bound state $|v=21\rangle$.

VI. CONCLUSION

In this work we have investigated the laser-controllable state-selective preparation of isolated diatomic molecules in specified vibrational bound states, up to the dissociation threshold of the electronic ground state, and the laser-controllable state-selective excitation of the continuum states from selectively prepared bound states on a femtosecond and picosecond time scale. In the stage of the bound states preparation our aim has been to achieve maximal state-selectivity along with minimizing the dissociation probability. In the stage of dissociation the aim has been to achieve maximal dissociation probability and selective control for the excitation of continuum states.

As a model system we have considered a one-dimensional dissociative Morse oscillator. The molecular dipole moment operator has been represented by the well-known Mecke function. The interaction with the laser field has been treated semiclassically: quantum molecule in a classical electric field. The general nature of the model implies that the tools of state-selective laser control similar to those described in this work can be developed for other diatomic molecules. Specific parameters of the model used in our computer simulations have been chosen to represent the local OH bond in the H_2O and HOD molecules.

The role of molecular rotation, which has not been taken into account in this work, requires special investigation (for the discussion of the relevance of one-dimensional to full-dimensional simulations for diatomic molecules see Ref. 41). However, the concept of vibrational excitation can be carried over from the one-dimensional to the three-dimensional case, especially because the control by linearly polarized fields already induces some degree of alignment.[77,78]

Basically, molecular rotation should be slow enough as compared to the rate of the laser controlled molecular preparation and dissociation, because it results in deviation of the electric field strength along the molecular dipole from the optimal value. In the stage of state-selective preparation, this will decrease the final population of the target level (for example, level $v=15$ in Figs. 2 and 3) and increase final populations of intermediate resonant levels ($v=5$ and 10). Nonresonant bound states will not acquire substantial final population, as it follows from the optimization procedure which is illustrated in Fig. 7(a) for the $|15\rangle \rightarrow |19\rangle$ transition. In the stage of dissociation, the role of rotation can be compensated by making use of stronger laser fields, due to monotonous increase of the dissociation probability with increasing laser field strength, see Fig. 5(b) and Fig. 8(c), for example.

A favourable system for a basic application of the tools of state-selective laser control developed here may be a mol-

ecule adsorbed on a surface, where the role of rotation and orientation is diminished.

Our computer simulations have been based on the direct numerical solution of the time-dependent Schrödinger equation by making use of a split time propagation (STP) method, and on the approximate approach of integro-differential equations (IDE) for the probability amplitudes of the bound states only, neglecting the laser-induced continuum–continuum transitions. The IDE approach is computationally less demanding than the exact STP method, therefore all optimizations of the controlling laser fields have been carried out within the IDE approach and afterwards checked by making use of the STP method. Good agreement between the results obtained by the IDE and STP methods show that the less demanding IDE approach can be used for simulations of the molecular quantum dynamics, at least as a first approximation. The IDE approach is based on the availability of the dipole matrix elements for the bound–continuum transitions which have been evaluated in this work in an analytical form suitable for program implementation. Combination of the two approaches proved to be suitable for revealing mechanisms underlying selective excitation of the continuum states, for analysing the processes of multiphoton and 1-photon above-threshold dissociation (ATD) in a single electronic state, and for designing the optimal laser fields for state-selective steering a molecule to a specified target in the discrete and in continuum spectrum.

The results obtained in this work show that a nonrotating diatomic molecule can be prepared on a fs/ps time scale in any prescribed vibrational bound state, including the very top one, with the state-selectivity approaching the maximal value $\mathscr{S}_v=1$. The controlling laser field may include several properly optimized sequential or overlapping ultrashort infrared laser pulses. State-selective preparation of the very top vibrational bound state may be accompanied by the appearance of an overexcited quasi-bound molecular state in the continuum, with a noticeable probability for the kinetic energy of fragments being equal to zero. The signature of this process is the appearance of the zero-order peak in the dissociation spectrum.

The laser-induced dissociation from selectively prepared intermediate bound states may be very efficient, with the dissociation probability approaching the maximal value $\mathscr{D}=1$ for a multiphoton pumping which yields typical ATD spectra. Direct 1-photon dissociation from selectively prepared bound vibrational states by making use of properly optimized sequential laser pulses enables one to achieve a flexible state-selective control of the dissociation spectra, implying time-selective and space-selective control of the dissociation products.

ACKNOWLEDGMENTS

We would like to thank Professor J. Manz for helpful discussions and Dr. Yu. A. Logvin for several STP simulations of the molecular dynamics. Generous support by the Volkswagen-Stiftung, Project No. I/69 348, is gratefully acknowledged. The computer simulations were carried out on HP 9000/S 750 workstations at the Freie Universität Berlin.

APPENDIX: BOUND–CONTINUUM COUPLINGS FOR A MORSE OSCILLATOR WITH MECKE DIPOLE FUNCTION

Generalized matrix elements in discrete and continuum states for the Morse oscillator have been evaluated in Ref. 79. Unfortunately, the results presented therein for the bound–continuum transitions are not suitable for program implementation. Therefore, we present below the derivation of matrix elements

$$\langle n|(r-r_0)\exp[-\lambda(r-r_0)]|E\rangle, \tag{A1}$$

which have been used in our IDE simulations. For the sake of completeness we also include some general results for the discrete and continuum spectra of the Morse oscillator.

The one-dimensional Morse potential, see Eq. (2), in dimensionless variables

$$x=(r-r_0)/r_0, \quad -1\leqslant x<\infty \tag{A2}$$

is written as

$$V(x)=D[\exp(-2\alpha x)-2\exp(-\alpha x)], \tag{A3}$$

where $\alpha=\beta r_0$. As is well known, see, e.g., Ref. 57, it admits exact solution of the time-independent Schrödinger equation

$$\frac{d^2\psi(x)}{dx^2}+[2\gamma^2\exp(-\alpha x)-\gamma^2\exp(-2\alpha x)]\psi(x) = \sigma^2\psi(x), \tag{A4}$$

where

$$\gamma^2=2mr_0^2D/\hbar^2, \quad \sigma^2=-2mr_0^2E/\hbar^2. \tag{A5}$$

Transformation to the new variables

$$y=2d\exp(-\alpha x), \quad d=\gamma/\alpha, \tag{A6}$$

and taking for the solution

$$\psi(y)=\exp(-y/2)y^{\sigma/\alpha}F(y), \tag{A7}$$

yields finally Kummer's standard form of the confluent hypergeometric equation

$$y\frac{d^2F}{dy^2}+(c-y)\frac{dF}{dy}-aF=0, \tag{A8}$$

where

$$c=(2\sigma/\alpha)+1; \quad a=(\sigma/\alpha)+0.5-d. \tag{A9}$$

Therefore, the general solution of Eq. (A4) is

$$\psi(y)=\exp(-y/2)y^{\sigma/\alpha}[A_1\Phi(a,c;y) + A_2y^{1-c}\Phi(a-c+1,2-c;y)], \tag{A10}$$

where y is defined by Eq. (A6), and $\Phi(a,c;y)$ is the confluent hypergeometric function.[80]

For the discrete spectrum, $E<0$ and $\sigma>0$, the boundary condition at $x\to\infty$ or $y=0$ requires $A_2=0$. The boundary

condition at $x=-1$ or $y=2d\ \exp(\alpha)\gg 1$ with the use of the asymptotic expansion for $\Phi(a,c;y)$ at $y\to\infty$, see Ref. 80, results in

$$a=-n,\quad n=0,1,2,\ \ldots N\leqslant(d-0.5), \tag{A11}$$

with $c=-2n+2d$, and finally gives eigenenergies

$$E_n=-D+\hbar[\omega_e(n+0.5)-\Delta^a(n+0.5)^2], \tag{A12}$$

where the harmonic frequency $\omega_e=(\alpha/r_0)\sqrt{2D/m}$, and the anharmonicity constant $\Delta^a=\hbar\omega_e^2/4D$. The confluent hypergeometric function reduces to the associated Laguerre polynomial,[81] and the eigenfunctions of the discrete states take the form

$$\psi_n(y)=N_n\ \exp(-y/2)y^{S_n/2}L_n^{S_n}(y), \tag{A13}$$

where $S_n=2d-2n-1$ and the normalization constant is

$$N_n=[\alpha(2d-2n-1)n!/\Gamma(2d-n)]^{1/2}. \tag{A14}$$

For the continuum spectrum, $E>0$, it is suitable to set $\sigma=i\varepsilon$, then from Eqs. (A5) and (A9) one has

$$\varepsilon^2=2mr_0^2E/\hbar^2;\quad E>0, \tag{A15}$$

and

$$c=i(2\varepsilon/\alpha)+1;\quad a=i(\varepsilon/\alpha)+0.5-d, \tag{A16}$$

with the following relations for the respective complex conjugates:

$$a^*=a-c+1;\quad c^*=2-c. \tag{A17}$$

The general solution (A10) takes the form

$$\psi(y)=\ \exp(-y/2)[A_1y^{i\varepsilon/\alpha}\Phi(a,c;y) + A_2y^{-i\varepsilon/\alpha}\Phi(a^*,c^*;y)]. \tag{A18}$$

The boundary condition at $x=-1$ or $y=2d\ \exp(\alpha)\gg 1$ with the use of the asymptotic expansion

$$\Phi(a,c;y)=\frac{\Gamma(c)}{\Gamma(a)}e^yy^{a-c}[1+\mathcal{O}(|y|^{-1})] \tag{A19}$$

at $y\to\infty$, where $\Gamma(z)$ is the gamma function,[80] result in

$$A_1=\Gamma(1-c)/\Gamma(a-c+1),\quad A_2=\Gamma(c-1)/\Gamma(a). \tag{A20}$$

From Eqs. (A18) and (A20) one can get eigenfunctions

$$\psi(E,y)=N(E)e^{-y/2}y^{i\varepsilon/\alpha}\Psi(a,c;y), \tag{A21}$$

where $\Psi(a,c;y)$ is the Ψ function.[80] Eigenfunctions (A21) die rapidly at $x\to-\infty$. The equivalent representation in terms of the Whittaker function,[80]

$$\psi(E,y)=N(E)y^{-1/2}W_{d,i\varepsilon/\alpha}(y), \tag{A22}$$

is more suitable for evaluating matrix elements for bound–continuum transitions.

The normalization constant $N(E)$ is obtained as follows. Assuming that the main input in the normalization integral

$$I(E',E)=\int_{-1}^{\infty}\psi(E',x)^*\psi(E,x)dx \tag{A23}$$

results from the domain of $x\to\infty$ or $y\to 0$, we keep only the first term in the expansion

$$\Phi(a,c,y)=1+(a/c)y+\mathcal{O}(|y|^2) \tag{A24}$$

at $y\to 0$, see Ref. 80. Then, the eigenfunctions in the x variable (A2) have the form

$$\psi(E,x)=N(E)[A_1(2d)^{i\varepsilon/\alpha}e^{i\varepsilon x}+A_2(2d)^{-i\varepsilon/\alpha}e^{-i\varepsilon x}], \tag{A25}$$

where A_1 and A_2 are given by Eqs. (A20). Evaluation of the normalization integral (A23) with $\psi(E,x)$ defined by Eq. (A25) yields

$$I(E',E)=N(E')^*N(E)A_1A_2\,2\pi\delta(\varepsilon'-\varepsilon), \tag{A26}$$

where δ is the Dirac delta-function. Taking into account the relation

$$\delta(\varepsilon'-\varepsilon)=2|\varepsilon|\,\delta(\varepsilon'^2-\varepsilon^2)-\delta(\varepsilon'+\varepsilon), \tag{A27}$$

and $\delta(\varepsilon'+\varepsilon)=0$ at $\varepsilon'>0$ and $\varepsilon>0$, one finally can get from Eq. (A26) the normalization constant

$$N(E)=\frac{r_0}{\hbar}\sqrt{\frac{m}{2\pi\varepsilon}}\frac{\Gamma(0.5-d-i\varepsilon/\alpha)}{\Gamma(-2i\varepsilon/\alpha)}. \tag{A28}$$

The normalization constant (A28) differs from that of Ref. 79, but agrees with the results of Ref. 82.

The dipole matrix elements for the bound-continuum transitions are evaluated as follows. The dipole moment function (7) in the dimensionless variable x (A2) has the form

$$\mu(x)=\mu_0r_0(x+1)\exp[-(x+1)r_0/r^0], \tag{A29}$$

and the matrix elements in question at real $\psi_n(x)$ are

$$\langle n|\mu|E\rangle=\int_{-1}^{\infty}\psi_n(x)\mu(x)\psi(E,x)dx. \tag{A30}$$

Transformation to variable $y=2d\ \exp(-\alpha x)$, see Eq. (A6), yields

$$\langle n|\mu|E\rangle=\int_0^{\infty}\psi_n(y)\mu(y)\psi(E,y)\frac{dy}{\alpha y}, \tag{A31}$$

where the dipole function $\mu(y)$ is obtained by making use of the relations

$$\ln y=\ \ln(2d)-\alpha x;\quad y^{\lambda}\ \ln y=(d/d\lambda)y^{\lambda}, \tag{A32}$$

yielding

$$\mu(y)=(\mu_0r_0/\alpha y_0^{\lambda})\{[\ln(2d)+\alpha]y^{\lambda}-(d/d\lambda)y^{\lambda}\}, \tag{A33}$$

where $\lambda=r_0/\alpha r^0$ and $y_0=2d\ \exp(\alpha)$. Finally we get the following representation for the matrix elements:

$$\langle n|\mu|E\rangle=\frac{\mu_0r_0}{\alpha^2y_0^{\lambda}}\left\{[\ln(2d)+\alpha]I(n,E;\lambda) - \frac{d}{d\lambda}I(n,E;\lambda)\right\}, \tag{A34}$$

where we have introduced the integral

$$I(n,E;\lambda)=\int_0^\infty \psi_n(y)y^{\lambda-1}\psi(E,y)dy, \tag{A35}$$

containing parameter λ, and we have changed the order of integration over y and differentiation over λ. The integral (A35) is evaluated by making use of the expansion of the associated Laguerre polynomials[81]

$$L_n^{S_n}(y)=\sum_{k=0}^{n} C_{k,n}y^k, \tag{A36}$$

where $C_{k,n}$ are defined as

$$C_{k,n}=\frac{(-1)^k}{k!}\binom{n+S_n}{n-k}. \tag{A37}$$

This yields the eigenfunctions of the discrete spectrum

$$\psi_n(y)=N_n e^{-y/2}y^{S_n/2}\sum_{k=0}^{n} C_{k,n}y^k, \tag{A38}$$

and, correspondingly, the parametric integral (A35)

$$I(n,E;\lambda)=N_n N(E)\sum_{k=0}^{n} C_{k,n}I_k(n,E;\lambda), \tag{A39}$$

where

$$I_k(n,E;\lambda)=\int_0^\infty e^{y/2}y^{S_n/2+\lambda+k-3/2}W_{d,i\varepsilon/\alpha}(y)dy. \tag{A40}$$

The integral (A40) is tabulated,[66] and one gets

$$I_k(n,E;\lambda)=\frac{|\Gamma(S_n/2+\lambda+k+i\varepsilon/\alpha)|^2}{\Gamma(\lambda-n+k)}. \tag{A41}$$

In a similar way we obtain

$$\frac{d}{d\lambda}I(n,E;\lambda)=N_n N(E)\sum_{k=0}^{n} C_{k,n}\frac{d}{d\lambda}I_k(n,E;\lambda). \tag{A42}$$

From Eq. (A41) one can get by differentiation:

$$\frac{d}{d\lambda}I_k(n,E;\lambda)=I_k(n,E;\lambda)\{2\mathrm{Re}[\psi(S_n/2+\lambda+k+i\varepsilon/\alpha)] - \psi(\lambda-n+k)\}, \tag{A43}$$

where $\psi(z)$ is the logarithmic derivative of the gamma function: $\psi(z)=\Gamma(z)^{-1}(d\Gamma(z)/dz)$, and Re[. . .] stands for the real part.

Dipole matrix elements for the bound–continuum transitions evaluated from Eq. (A34) with making use of Eqs. (A37), (A39), (A41)–(A43) and (A14), (A28) have been used in our IDE simulations.

[1] N. Bloembergen and A. H. Zewail, J. Phys. Chem. **88**, 5459 (1984).
[2] *Multi-Photon Excitation and Dissociation of Polyatomic Molecules*, edited by C. D. Cantrell (Springer, Berlin,1986).
[3] D. W. Lupo and M. Quack, Chem. Rev. **87**, 181 (1987).
[4] *Atomic and Molecular Processes with Short Intense Laser Pulses*, edited by A. D. Bandrauk (Plenum, New York, 1988).
[5] P. Brumer and M. Shapiro, Annu. Rev. Phys. Chem. **43**, 257 (1992).
[6] M. Quack and J. Stohner, J. Phys. Chem. **97**, 12574 (1993).
[7] P. M. Felker and A. H. Zewail, in *Femtosecond Chemistry*, edited by J. Manz and L. Wöste (Verlag Chemie, Weinheim, 1995), Vol. 1, pp. 193–260.
[8] B. Amstrup, R. J. Carlson, A. Matro, and S. A. Rice, J. Phys. Chem. **95**, 8019 (1991).
[9] W. S. Warren, H. Rabitz, and M. Dahleh, Science **259**, 1581 (1993).
[10] A. H. Zewail, in *Femtosecond Chemistry*, edited by J. Manz and L. Wöste (Verlag Chemie, Weinheim, 1995), Vol. 1, pp. 15–130.
[11] J. Manz and C. S. Parmenter, Chem. Phys. **139**, 1 (1989).
[12] R. Marquardt and M. Quack, J. Chem. Phys. **95**, 4854 (1991).
[13] S. Shi and H. Rabitz, Comp. Phys. Commun. **63**, 71 (1991).
[14] C. D. Schwieters and H. Rabitz, Phys. Rev. A **44**, 5224 (1991).
[15] G. K. Paramonov and V.A Savva, Phys. Lett. A **97**, 340 (1983).
[16] G. K. Paramonov, V. A. Savva, and A. M. Samson, Infrared Phys. **25**, 201 (1985).
[17] G. K. Paramonov, Phys. Lett. A **152**, 191 (1991).
[18] R. Judson, K. Lehmann, W. S. Warren, and H. Rabitz, J. Mol. Struct. **223**, 425 (1990).
[19] W. Jakubetz, B. Just, J. Manz, and H.-J. Schreier, J. Phys. Chem. **94**, 2294 (1990).
[20] W. Jakubetz, J. Manz, and H.-J. Schreier, Chem. Phys. Lett. **165**, 100 (1990).
[21] B. Just, J. Manz, and G. K. Paramonov, Chem. Phys. Lett. **193**, 429 (1992).
[22] U. Gaubatz, P. Rudecki, S. Schiemann, and K. Bergmann, J. Chem. Phys. **92**, 5363 (1990).
[23] B. W. Shore, K. Bergmann, J. Oreg, and S. Rosenwaks, Phys. Rev. A **44**, 7442 (1991).
[24] J. Oreg, K. Bergmann, B. W. Shore, and S. Rosenwaks, Phys. Rev. A **45**, 4888 (1992).
[25] B. W. Shore, K. Bergmann, A. Kuhn, S. Schiemann, J. Oreg, and J. H. Eberly, Phys. Rev. A **45**, 5297 (1992).
[26] Y. J. Yan, R. E. Gillian, R. M. Whitnell, K. R. Wilson, and S. Mukamel, J. Phys. Chem. **97**, 2320 (1993).
[27] B. Kohler, J. L. Krause, F. Raksi, C. Rose-Petruck, R. M. Whitnell, K. R. Wilson, V. V. Yakovlev, and Y. J. Yan, J. Phys. Chem. **97**, 12602 (1993).
[28] J. L. Krause, R. M. Whitnell, K. R. Wilson, and Y. J. Yan, J. Phys. Chem. **99**, 6562 (1993).
[29] J. L. Krause, R. M. Whitnell, K. R. Wilson, and Y. Yan, *Femtosecond Chemistry*, edited by J. Manz and L. Wöste (Verlag Chemie, Weinheim, 1995), Vol. 2, pp. 743–780.
[30] J. S. Melinger, S. R. Gandhi, A. Hariharan, J. X. Tull, and W. S. Warren, Phys. Rev. Lett. **68**, 2000 (1992).
[31] J. E. Combariza, J. Manz, and G. K. Paramonov, Faraday Discuss. Chem. Soc. **91**, 358 (1991).
[32] J. E. Combariza, B. Just, J. Manz, and G. K. Paramonov, J. Phys. Chem. **95**, 10351 (1991).
[33] J. Combariza, S. Görtler, B. Just, and J. Manz, Chem. Phys. Lett. **195**, 393 (1992).
[34] J. E. Combariza, C. Daniel, B. Just, E. Kades, E. Kolba, J. Manz, W. Malisch, G. K. Paramonov, and B. Warmuth, in *Isotope Effects in Gas-Phase Chemistry*, edited by J. E. Kaye (American Chemical Society, Washington D.C., 1992), pp. 310–334.
[35] A. E. Bryson and Y. Ho, *Applied Optimal Control* (Hemisphere, New York, 1975).
[36] S. Shi, A. Woody, and H. Rabitz, J. Chem. Phys. **88**, 6870 (1988).
[37] A. P. Pierce, M. A. Dahleh, and H. Rabitz, Phys. Rev. A **37**, 4950 (1988).
[38] S. Shi and H. Rabitz, J. Chem. Phys. **92**, 2927 (1990).
[39] M. A. Dahleh, A. P. Pierce, and H. Rabitz, Phys. Rev. A **42**, 1065 (1990).
[40] P. Gross, D. Neuhauser, and H. Rabitz, J. Chem. Phys. **98**, 4557 (1993).
[41] M. Kaluža, T. Muckerman, P. Gross, and H. Rabitz, J. Chem. Phys. **100**, 4211 (1994).
[42] Y. He, M. Quack, R. Ranz, and G. Seyfang, Chem. Phys. Lett. **215**, 228 (1993).
[43] S. Chelkowski, A. D. Bandrauk, and P. B. Corkum, Phys. Rev. Lett. **65**, 2355 (1990).
[44] B. Just, J. Manz, and J. Trisca, Chem. Phys. Lett. **193**, 423 (1992).
[45] W. Jakubetz, E. Kades, and J. Manz, J. Phys. Chem. **97**, 12609 (1993).
[46] J. Manz and G. K. Paramonov, J. Phys. Chem. **97**, 12625 (1993).
[47] W. Gabriel and P. Rosmus, J. Phys. Chem. **97**, 12644 (1993).
[48] H.-P. Breuer and M. Holthaus, J. Phys. Chem. **97**, 12634 (1993).
[49] G. K. Paramonov, in *Femtosecond Chemistry*, edited by J. Manz and L. Wöste (Verlag Chemie, Weinheim, 1995), Vol. 2, pp. 671–712.
[50] C. Leforestier and R. E. Wyatt, J. Chem. Phys. **78**, 2334 (1983).

[51] C. Leforestier and R. E. Wyatt, J. Chem. Phys. **82**, 752 (1984).
[52] C. Leforestier and R. E. Wyatt, Chem. Phys. **98**, 123 (1985).
[53] T. M. Flosnik and R. E. Wyatt, Phys. Rev. A **40**, 5716 (1989).
[54] M. E. Goggin and P. W. Milonni, Phys. Rev. A **37,** 796 (1987).
[55] M. E. Goggin and P. W. Milonni, Phys. Rev. A **38**, 5174 (1988).
[56] J. H. Shirley, Phys. Rev. **138**, 979 (1965).
[57] S. Flügge, *Practical Quantum Mechanics* (Springer, New York, 1974).
[58] M. L. Sage, Chem. Phys. **35**, 375 (1978).
[59] J. T. Broad, Phys. Rev. A **26**, 3078 (1982).
[60] R. Mecke, Z. Elektrochem. **54**, 38 (1950).
[61] R. T. Lawton and M. S. Child, Mol. Phys. **40**, 773 (1980).
[62] M. D. Feit, J. A. Fleck, and A. Steiger, J. Comput. Phys. **47**, 412 (1982).
[63] M. D. Feit and J. A. Fleck, J. Chem. Phys. **78**, 301 (1982).
[64] M. D. Feit and J. A. Fleck, J. Chem. Phys. **80**, 2578 (1984).
[65] R. N. Bisseling, R. Kosloff, and J. Manz, J. Chem. Phys. **83**, 993 (1985).
[66] I. S. Gradshteyn and I. M. Ryzhik, *Table of Integrals, Series, and Products* (Academic, New York, 1980).
[67] W. H. Press, B. P. Flannery, S. A. Teukolsky, and W. T. Vetterling, *Numerical Recipes* (Cambridge University Press, Cambridge, 1986).
[68] T. Joseph and J. Manz, Mol. Phys. **58**, 1149 (1986).
[69] A. D. Bandrauk and N. Gélinas, in *Atomic and Molecular Processes with Short Intense Laser Pulses*, edited by A. D. Bandrauk (Plenum, New York, 1988), pp. 263–272.
[70] A. D. Bandrauk and J. M. Gauthier, J. Opt. Soc. Am. B **7**, 1420 (1990).
[71] X. He and O. Atabek, Phys. Rev. Lett. **64**, 515 (1990).
[72] P. H. Bucksbaum, A. Zavriyev, H. G. Muller, and D. W. Schumacker, Phys. Rev. Lett. **64**, 1883 (1990).
[73] A. Zavriyev, P. H. Bucksbaum, J. Squier, and S. Saline, Phys. Rev. Lett. **70**, 1077 (1993).
[74] H. Yang and J. L. Whitten, Surf. Sci. **223**, 131 (1989).
[75] K. Müller-Dethlefs and E. W. Schlag, Annu. Rev. Phys. Chem. **42**, 109 (1991).
[76] M. Quack, in *Femtosecond Chemistry*, edited by J. Manz and L. Wöste (Verlag Chemie, Weinheim, 1995), Vol. 2, pp. 781–818.
[77] B. Friedrich and D. Herschbach, Phys. Rev. Lett. **74**, 4623 (1995).
[78] T. Seideman, J. Chem. Phys. **103**, 7887 (1995).
[79] A. Matsumoto, J. Phys. B: At. Mol. Opt. Phys. **21**, 2863 (1988).
[80] Bateman Manuscript Project, *Higher Transcendental Functions*, edited by A. Erdélyi (McGraw-Hill, New York, 1953), Vol. 1.
[81] Bateman Manuscript Project, *Higher Transcendental Functions*, edited by A. Erdélyi (McGraw-Hill, New York, 1953), Vol. 2.
[82] C. Haug, W. Brenig, and T. Brunner, Surf. Sci. **227**, 167 (1990).